I. NUMERICAL SOLUTION OF THE SUPERFLUID SHOCK JUMP CONDITIONS
II. EXPERIMENTAL INVESTIGATION OF THE LIQUID HELIUM II - VAPOR INTERFACE

Thesis by
Douglas Marion Moody, Jr.

In Partial Fulfillment
of the Requirements for the Degree of
Doctor of Philosophy

California Institute of Technology
Pasadena, California

1983
(Submitted 6 May 1983)

To my mother and

the memory of my father.

ACKNOWLEDGEMENTS

I would like to thank Professor Hans W. Liepmann for giving me the opportunity to return to Caltech and study with him. I am particularly grateful for his suggesting a change of direction to the computations which comprise Part I, and for his patience once this change was made. I also thank Professor Bradford Sturtevant for guidance in developing the computer program which produced the results of Part I and for his suggested revisions after carefully reading the first versions of this thesis.

Among the many GALCIT staff members who very willingly provided their help over the last few years, I am especially indebted to Messrs George Lundgren and Robert Seguine of the Aeronautics Shop for many hours of instruction on machining techniques and to Mrs. Jacquelyn Beard for help in text processing the manuscript.

Finally, to all of my fellow GALCIT graduate students, whom it has been a great pleasure to know, I extend my thanks for their friendship and for many technical discussions and suggestions.

NUMERICAL SOLUTION OF THE SUPERFLUID HELIUM SHOCK JUMP CONDITIONS

ABSTRACT

The four fundamental conservation equations of superfluid mechanics may be integrated across a one-dimensional discontinuity (shock wave) propagating into undisturbed helium II to yield a set of four algebraic equations (jump conditions) which, when supplemented by thermodynamic state information, establish the equilibrium flow state behind the shock wave for a given wave speed and undisturbed flow state ahead of the shock. These jump conditions have been solved numerically for 19 points on the helium II p-T diagram with upstream Mach number as the independent parameter. Representative results of the calculations are presented for pressure shocks, temperature raising shocks, and temperature lowering shocks. The results are compared to previous analytical approximate solutions to test the validity of those approximations. They are also compared to experimental data for shock waves in helium II as a means of testing the correctness of the full, nonlinear two-fluid equations.

EXPERIMENTAL INVESTIGATION OF THE LIQUID HELIUM II - VAPOR INTERFACE

ABSTRACT

An apparatus was designed and constructed to measure the linear reflection and transmission coefficients for weak second sound shocks impinging upon the liquid-vapor interface of helium II. The measured reflection coefficients reproduce the work of previous authors, giving values which are roughly 20% higher than those predicted by thermodynamic equilibrium theory. The transmitted pressure wave speed was measured, and was found to be sonic within the limits of experimental precision. Therefore strength could not be deduced from time of flight measurements. Direct amplitude measurements of this weak wave were prevented by the film which coats the sensors in the vapor. For these reasons, the attempted transmission coefficient measurements were unsuccessful.

TABLE OF CONTENTS

LIST OF FIGURES

LIST OF TABLES

PART I

NUMERICAL SOLUTION OF THE SUPERFLUID SHOCK JUMP CONDITIONS

Chapter 1

INTRODUCTION

This work was undertaken as an attempt to shed light upon the implications of data from experiments on shock waves in superfluid helium. The data provide a means of testing the correctness of the nonlinear two-fluid equations if the shock jump conditions which follow from these equations can be solved. But due to the complexity of these jump conditions and the associated superfluid thermodynamics, closed form analytical solutions are not possible, and only approximations for weak shocks have heretofore been obtained. The experimental shock wave data in some cases show significant disagreement with these approximations, and an important question then arises. Are the disagreements a consequence of the weak wave approximation; or, more fundamentally, do they indicate a failure of the two-fluid model? A natural approach to resolving this question is to seek numerical solutions of the jump conditions which are limited in quality only by the quality of existing helium II thermodynamic data.

Current limitations on the quality of helium II thermodynamics stem from two sources. The pressure and temperature dependences of the state variables are known from sound speed data to a precision of approximately 0.3%. More importantly, dependence of the state variables on the counterflow velocity w can only be approximated at this time by neglecting the w dependence of the normal fluid fraction. The resulting leading order corrections for chemical potential, entropy, and density are then valid only for the case of w small.

Comparison of the numerical results to pressure shock data shows good agreement for experiments at temperatures below 1.88 °K. Disagreements above 1.88 °K are probably due to evaporative effects. Comparison to temperature shock data shows agreement for low Mach numbers but significant disagreement at higher Mach numbers. The higher Mach number temperature shock data can possibly be used to improve the two-fluid thermodynamics.

Before discussing the shock jump conditions and their solutions, a brief introduction is given on the physical properties of helium II which motivate a two-fluid model and on the Landau equations which express this model mathematically. Discussions then follow on linear wave propagation and shock waves in helium II. The chapter concludes with a section describing previous superfluid shock wave experiments.

1.1. Physical Basis for the Two-Fluid Model of Helium

At low temperatures, helium exhibits a number of remarkable properties and behaviors which are unique among all substances encountered in nature. These properties are all ultimately the consequences of two features of the ^{4}He atom -- a high degree of symmetry and a low atomic mass. The atom in its ground state has the most stable and symmetric of electronic configurations. The two electrons are spin paired in the 1s level. (Thermal excitations from the atomic ground state can only be expected at temperatures exceeding $10^5\ ^0$K.) As a result the atom is very resistant to polarization, giving rise to exceedingly small classical potential interactions (van der Waals' forces) with any neighboring atom. For this reason helium is the most difficult gas to liquefy. Its boiling point is 4.21 ^{0}K at one atmosphere. Thinking in purely classical terms, one could say the helium atom is nature's most perfect hard sphere -- the kinetic theorist's dream. Quantum mechanically speaking however, the high degree of symmetry plays a quite different role. The ground state is characterized by complete spin pairing of the atom's nucleons as well as its electrons. One can therefore say from a quantum statistical viewpoint that among particles in nature which have non-zero mass the helium atom is the lightest most perfect boson. The small mass leads to a large deBroglie wavelength for the atom at low temperatures (Λ = 7.6 Å at 4.21 ^{0}K). Thus, observing a collection of ^{4}He atoms, one might expect to see evidence of Bose attraction (the tendency of symmetric wave functions to overlap) and ultimately Bose condensation as Λ becomes comparable to the spacing between atoms. In fact as liquid helium is cooled along its vapor pressure curve, it undergoes a second-order phase transition at 2.17 ^{0}K to a distinct liquid phase (deemed helium II) which exhibits many remarkable properties, some of which are discussed below. This phase transition is called the lambda transition, and although certainly a manifestation of wave function overlap, it is dissimilar in many respects to the perfect gas Bose condensation of

point mass particles (see for example, Goodstein, Chapter 5).

Helium II is remarkable in that heat is reversibly transported in this liquid by convection. As a result, temperature disturbances propagate as waves called "second sound". The name second sound is intended to indicate a wavelike behavior in addition to the ordinary acoustic one (called first sound in helium II) associated with pressure disturbances. The helium II phase is sometimes called superfluid, owing to its ability to flow through fine capillaries with no pressure loss. This might lead one to conclude that helium II has zero viscosity. However, a body moving through helium II will experience a viscous drag. For example, a torsional pendulum consisting of an oscillating thin flat plate will be damped in helium II, and the damping time will increase as the liquid temperature is decreased. This result seems to indicate a non-zero viscosity which decreases with temperature. These apparently contradictory results of capillary and torsional pendulum experiments led historically to the proposal of a two-fluid model for helium II. In this model the fluid is imagined to consist of two components. One is responsible for viscous interactions and is called normal. The other, called super, is able to flow inviscidly and is a macroscopic manifestation of a single quantum mechanical collective ground state. This ground state is in some ways analagous to that occupied by the Bose condensate of perfect gas of bosons. Since the super component represents a single microstate, it has zero entropy. The experimental results are now resolved as follows. Within the capillary, the normal fluid is clamped by viscosity, but the super component, completely lacking viscosity, flows through freely. The pendulum on the other hand is damped by interaction with the normal component only. The mass fractions of super and normal fluids ($\frac{\rho_s}{\rho}$ and $\frac{\rho_n}{\rho}$) vary with temperature but always sum to unity. At the lambda transition $\frac{\rho_n}{\rho}$ is unity and decreases smoothly to zero at absolute zero. Thus the damping of the pendulum is weaker

at lower temperatures since less normal fluid is present.

One further property of liquid helium, also the result of high symmetry and low atomic mass, should be mentioned. The liquid never freezes under its own vapor pressure, not even at absolute zero. This results from the high zero point energy which is inversely proportional to the atom's mass and the very small interatomic attractions caused by electronic orbital symmetry. The solid phase of ^{4}He can be reached by applying a pressure of approximately 25 atmospheres to the liquid.

1.2. The Landau Equations for the Two-Fluid Model

The mathematical formulation of the two-fluid model was given by Landau in 1941 (Landau, 1941; Landau & Lifshitz, 1959). The total fluid density is taken to be the sum of the super and normal component densities.

$$\rho = \rho_s + \rho_n \tag{1-1}$$

Now ρ_s represents the degree to which the liquid occupies a single quantum mechanical ground state, and ρ_n can therefore be identified as the density of collective excitations out of that state. Thus these component densities do not represent mass fractions in the sense of separable species. Separate velocity fields $\vec{u}_s$ and $\vec{u}_n$ are ascribed to the super and normal components respectively.

The super component's density and velocity can be more precisely related to the quantum mechanical ground state for the system by expressing the wave function for this state as

$$\psi(\vec{r},t) = [\rho_s(\vec{r},t)]^{\frac{1}{2}} e^{i\varphi(\vec{r},t)} \tag{1-2}$$

Thus the superfluid density is directly related to the amplitude of the wave function since

$$\rho_s = \psi^* \psi \tag{1-3}$$

Furthermore, the mass flux is given in terms of the current density established by the wave function's gradient.

$$\rho_s \vec{u}_s = \frac{\hbar}{2im} \left(\psi^* \nabla \psi - \psi \nabla \psi^* \right) \tag{1-4}$$

It follows that

$$\vec{u}_s = \frac{\hbar}{m} \nabla \varphi \tag{1-5}$$

where $\hbar$ denotes Planck's constant divided by 2π and m the total mass of the superfluid fraction. Thus as a consequence of a single, well-ordered ground state, the macroscopic flow of the superfluid is irrotational,

$$\nabla \times \vec{u}_s = 0 \tag{1-6}$$

and the phase of the wave function serves as the velocity potential.

Consider now the physical interpretation of the normal component mass flux as an excitation flux. To an observer moving with the super component (i.e., with velocity $\vec{u}_s$), this excitation flux is given by

$$\vec{j}_0 = \rho_n \vec{w} \tag{1-7}$$

where

$$\vec{w} = \vec{u}_n - \vec{u}_s \tag{1-8}$$

is the relative (or counterflow) velocity between the two components. (The zero subscript in this section is used to indicate the frame of reference in which the superfluid is at rest.) Now since all velocities must transform according to Galilean relativity, the mass flux in the lab-fixed frame is given by

$$\vec{j} = \rho \vec{u} = \rho(\vec{u}_s + \vec{u}_0) = \rho \vec{u}_s + \vec{j}_0 \tag{1-9}$$

From the physical meaning given to $\vec{j}_0$ by equation (1-7), it follows from (1-9) that

$$\rho \vec{u} = \rho_s \vec{u}_s + \rho_n \vec{u}_n \tag{1-10}$$

The concept embodied in (1-7) also requires the thermodynamic identity to be extended to include the energy contribution from the excitations. In the superfluid frame

$$dU_0 = TdS - pdV + \mu dM + \vec{w} \cdot d(V \vec{j}_0) \tag{1-11}$$

where the extensive quantities are

U_0 = internal energy

S = entropy

V = volume

M = mass

$V\vec{j}_0$ = momentum of excitations

and the intensive quantities are

T = temperature

p = pressure

μ = chemical potential per unit unit mass

$\vec{w}$ = velocity of excitations

Equation (1-11) can be looked upon as defining the excitation velocity $\vec{u}_n$ ($\vec{w}$ in the superfluid frame) as the derivative of energy with respect to momentum. An extended Gibbs-Duhem relation follows from (1-11).

$$Md\mu = -SdT + Vdp - V\vec{j}_0 \cdot d\vec{w} \tag{1-12}$$

The thermodynamic equations (1-11) and (1-12) may be rewritten as

$$d(\rho e_0) = Td(\rho s) + \mu d\rho + \vec{w} \cdot d\vec{j}_0 \tag{1-13}$$

$$d\mu = -sdT + \frac{1}{\rho}dp - \frac{\rho_n}{\rho}\vec{w} \cdot d\vec{w} \tag{1-14}$$

where e_0 and s represent the specific internal energy and the specific entropy respectively.

Equations (1-1),(1-8), and (1-10) may be combined to write

$$\vec{u}_n = \vec{u} + \frac{\rho_s}{\rho}\vec{w} \tag{1-15}$$

$$\vec{u}_s = \vec{u} - \frac{\rho_n}{\rho}\vec{w} \tag{1-16}$$

Before discussing the conservation equations which govern the flow of helium II, consider the quantities which specify an equilibrium (i.e., non-dissipative) flow state. Upon inspection of equation (1-14) it is clear that pressure, temperature, and magnitude of counterflow velocity may be chosen as the independent variables necessary to thermodynamically specify the state. Dynamically, the vectors $\vec{u}$ and $\vec{w}$ (or equivalently $\vec{u}_n$ and $\vec{u}_s$) are required. Therefore two vector and two scalar governing equations will be expected.

Conservation of mass requires the continuity equation to be obeyed.

$$\frac{\partial \rho}{\partial t} + \nabla \cdot \vec{j} = 0 \tag{1-17}$$

Conservation of momentum can be expressed generally as

$$\frac{\partial \vec{j}}{\partial t} + \nabla \cdot \overleftrightarrow{\Pi} = 0 \tag{1-18}$$

where the momentum flux density tensor $\overleftrightarrow{\Pi}$ is as yet unknown. Since only non-dissipative flows are currently being considered, entropy must be conserved. Thus

$$\frac{\partial (\rho s)}{\partial t} + \nabla \cdot \vec{F} = 0 \tag{1-19}$$

where $\vec{F}$ represents the entropy flux. One further vector equation is provided by recalling that the super component velocity field is irrotational. Thus the time derivative of $\vec{u}_s$ as well as $\vec{u}_s$ itself may be expressed as the gradient of some scalar function.

$$\frac{d\vec{u}_s}{dt} = -\nabla \Phi$$

Or, since $\nabla \times \vec{u}_s = 0$, this can be written as

$$\frac{\partial \vec{u}_s}{\partial t} + \nabla \left(\Phi + \frac{1}{2} u_s^2 \right) = 0 \tag{1-20}$$

Equations (1-17) through (1-20) govern the flow field but are only meaningful if $\overleftrightarrow{\Pi}, \vec{F}$, and Φ can be deduced. Landau accomplished this by requiring the conservation of energy equation to be satisfied

$$\frac{\partial E}{\partial t} + \nabla \cdot \vec{Q} = 0 \tag{1-21}$$

and requiring all velocities to Galilean transform from the superfluid rest frame to the lab frame. From these two requirements, it can be shown after laborious manipulation that

$$\overleftrightarrow{\Pi} = \rho_s \vec{u}_s \vec{u}_s + \rho_n \vec{u}_n \vec{u}_n + p\overleftrightarrow{I} \tag{1-22a}$$

$$= \rho \vec{u}\vec{u} + \frac{\rho_s \rho_n}{\rho} \vec{w}\vec{w} + p\overleftrightarrow{I} \tag{1-22b}$$

$$\vec{F} = \rho s \vec{u}_n \tag{1-22c}$$

$$\Phi = \mu \tag{1-22d}$$

$$E = \rho e_0 + \frac{1}{2}\rho u_s^2 + \rho_n \vec{w} \cdot \vec{u}_s \tag{1-22e}$$

$$\vec{Q} = (\mu + \frac{1}{2}u_s^2)\rho \vec{u} + \rho s T \vec{u}_n + \rho_n \vec{u}_n (\vec{u}_n \cdot \vec{w}) \tag{1-22f}$$

and the mass flux (equation 1-10) is

$$\vec{j} = \rho\vec{u} = \rho_s\vec{u}_s + \rho_n\vec{u}_n \tag{1-22g}$$

The Landau two-fluid formulation is now complete. Conservation of mass (1-17), momentum (1-18), and energy (1-21) together with the superfluid equation (1-20) form the complete set of equations for superfluid dynamics. If the flow of interest is dissipationless, the conservation of entropy equation (1-19) is equivalent to and may be used in place of the equation for conservation of energy.

The conservation equations are very complex since as indicated by equation (1-14) the thermodynamic state variables all depend on the counterflow speed w. Although the exact dependence is not currently known, it can be derived for the case of w small. In this limit, equation (1-14) implies

$$\tilde{\mu}(p,T,w^2) \approx \mu(p,T) - \frac{w^2}{2}\frac{\rho_n}{\rho} \tag{1-23}$$

where all quantities on the right hand side are functions of p and T only. The tilde will henceforth be used over state variables to denote this second-order dependence on the magnitude of the counterflow velocity. Entropy and density are then found by differentiating (1-23) with respect to temperature and pressure.

$$\tilde{s}(p,T,w^2) \approx s(p,T) + \frac{w^2}{2}\frac{\partial}{\partial T}\left[\frac{\rho_n}{\rho}\right] \tag{1-24}$$

$$\tilde{\rho}(p,T,w^2) \approx \rho(p,T) + \frac{\rho^2 w^2}{2}\frac{\partial}{\partial p}\left[\frac{\rho_n}{\rho}\right] \tag{1-25}$$

1.3. Sound Propagation in Helium II

The Landau equations predict the existence of the previously mentioned linear wave modes of first and second sound. Upon linearizing equations (1-17) through (1-20) we have

$$\frac{\partial \rho}{\partial t} + \rho_0 \nabla \cdot \vec{u} = 0 \tag{1-26}$$

$$\rho_0 \frac{\partial \vec{u}}{\partial t} + \nabla p = 0 \tag{1-27}$$

$$\rho_0 \frac{\partial s}{\partial t} + s_0 \frac{\partial \rho}{\partial t} + \rho_0 s_0 \nabla \cdot \vec{u}_n = 0 \tag{1-28}$$

$$\frac{\partial \vec{u}_s}{\partial t} + \nabla \mu = 0 \tag{1-29}$$

In this section, the zero subscript refers to the undisturded equilibrium state in which all velocities are zero. All non-subscripted variables represent small perturbations to that state, and in equations (1-26) through (1-29) only the terms which are linear in these perturbations have been retained. Combining the time derivative of (1-26) with the divergence of (1-27) yields

$$\frac{\partial^2 \rho}{\partial t^2} = \nabla^2 p \tag{1-30}$$

Using equations (1-15),(1-16), and the linearized version of (1-14), equations (1-28) and (1-29) may be combined to give

$$\frac{\partial^2 s}{\partial t^2} = \frac{\rho_{s_0}}{\rho_{n_0}} s_0^2 \nabla^2 T \tag{1-31}$$

The propagation of small pressure-density disturbances (first sound) is governed by the equation (1-30) while propagation of small temperature-entropy disturbances (second sound) is governed by the wave equation (1-31). These two linear wave modes are coupled to each other because the density will in general vary with temperature as well as with pressure while the entropy will vary with pressure as well as with temperature. This is to say coupling occurs through the coefficient of thermal expansion β defined as

$$\beta = -\frac{1}{\rho}\left(\frac{\partial \rho}{\partial T}\right)_p$$

Conversely, two independent wave motions (with two associated wave speeds) can be executed by the fluid in the approximation of zero thermal expansion. This is in fact a good approximation for helium II except very close to the lambda transition. From thermodynamics, lack of density variation with temperature (i.e., $\beta = 0$) implies lack of entropy variation with pressure

$$\left(\frac{\partial s}{\partial p}\right)_T = 0$$

and equivalence of constant pressure and constant volume specific heats.

$$\gamma = \frac{c_p}{c_v} = 1$$

It follows then that

$$d\rho = \left[\frac{\partial \rho}{\partial p}\right]_T dp = \left[\frac{\partial \rho}{\partial p}\right]_s dp$$

and that

$$ds = \left[\frac{\partial s}{\partial T}\right]_p dT = \left[\frac{\partial s}{\partial T}\right]_v dT$$

Since in the linear wave equations the variations of quantities from equilibrium are small enough to be taken as differentials, equations (1-30) and (1-31) can now be written in the uncoupled approximation as

$$\frac{\partial^2 \rho}{\partial t^2} = \alpha_1^2 \nabla^2 \rho \tag{1-32}$$

$$\frac{\partial^2 s}{\partial t^2} = \alpha_2^2 \nabla^2 s \tag{1-33}$$

where the speed of pure first sound is identified as

$$\alpha_1 = \left[\frac{\partial p}{\partial \rho}\right]_s^{\frac{1}{2}} \tag{1-34}$$

and the speed of pure second sound is identified as

$$\alpha_2 = \left[\frac{\rho_s s^2 T}{\rho_n c_p}\right]^{\frac{1}{2}} \tag{1-35}$$

1.4. Shock Waves in Helium II

Suppose pressure or temperature disturbances introduced into the liquid are of sufficient magnitude to invalidate the linear approximations made in the previous section. The neglected nonlinear terms in the dynamic and thermodynamic equations provide for the occurrence of wave steepening. Consider the propagation in one dimension (taken as the x-axis say) of a disturbance which initially has a smooth shape which slowly varies with x. Owing to nonlinear effects, the speed of propagation will be amplitude dependent. For example, it will be shown that in helium II, regions of higher density in a pressure disturbance will travel faster than those of lower density. A slowly rising compressive disturbance will therefore tend to steepen as it propagates and ultimately form a discontinuity or shock wave. The tendency toward further steepening, that is the overtaking of low density regions by higher density ones, is prevented by the dissipative processes of viscosity and heat conduction which occur within the shock. The shock wave therefore produces a very sharp (almost discontinuous) change of state across itself as it propagates into the fluid. The change is from one equilibrium flow state ahead to another behind the wave, and although dissipation occurs within the shock, the details of how it occurs need not be considered if the governing differential equations are integrated across the discontinuity to connect a point ahead of the shock to one behind it. That is, the Landau conservation equations of mass, momentum, superfluid motion, and energy (entropy is not conserved since the shock causes dissipation) should, when integrated across the shock, give the jump from the unshocked to the shocked flow state even though these equations contain no dissipative terms.

The integration of the differential equations is effected by transforming to a steady coordinate system. Consider a one dimensional shock wave propagating into undisturbed helium II with speed c (see Figure 1-1a), and from this lab-fixed coordinate system (denoted by f) transform to a system in which the shock

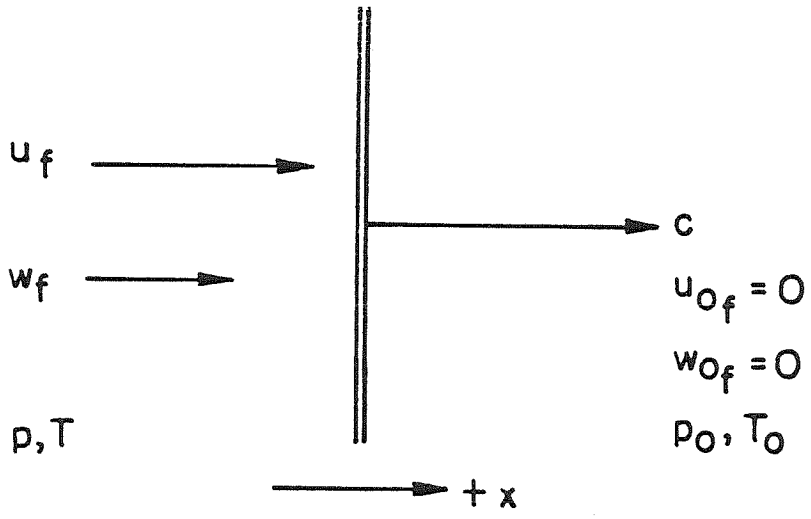

Figure 1-1a. Lab-Fixed Coordinates

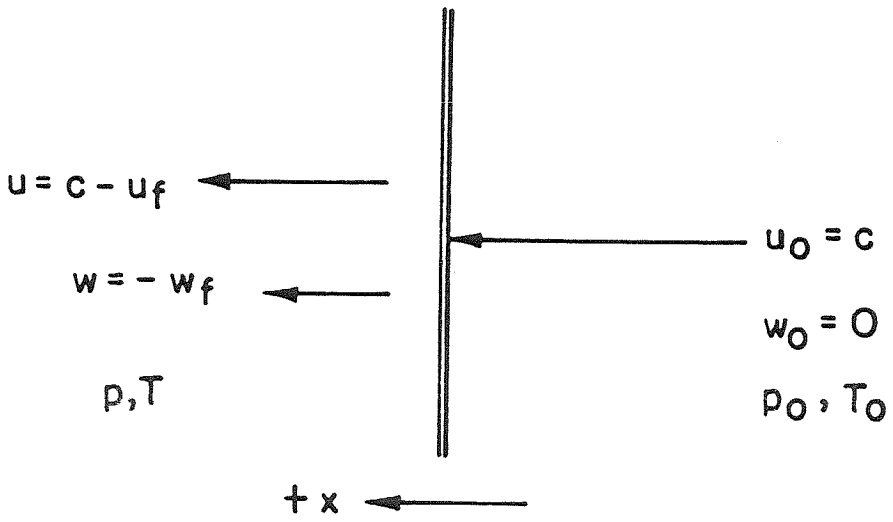

Figure 1-1b. Shock-Fixed Coordinates

is fixed (Figure 1-1b). In this section and hereafter, a zero subscript refers to unshocked fluid. Note that the relative velocity w is invariant under this transformation, and as a result, a conventionally positive relative velocity in lab-fixed coordinates (i.e., toward the shock) will be negative in the shock-fixed frame. Since the flow is steady in the shock-fixed frame, all time derivatives vanish. Integration of the equations for conservation of mass (1-17), momentum (1-18), superfluid motion (1-20), and energy (1-21) across the shock then gives

$$\tilde{\rho} u = \rho_0 u_0 \tag{1-36}$$

$$p + \rho_s u_s^2 + \rho_n u_n^2 = p_0 + \rho_0 u_0^2 \tag{1-37}$$

$$\tilde{\mu} + \frac{1}{2} u_s^2 = \mu_0 + \frac{1}{2} u_{s_0}^2 \tag{1-38}$$

$$\tilde{\rho}\,\tilde{s}\,T u_n + \rho_n u_n^2 w = \rho_0 s_0 T_0 u_{n_0} \tag{1-39}$$

where the fluxes have been identified using equations (1-22). Using equations (1-15) and (1-16) to eliminate u_n and u_s and then eliminating u by (1-36), we arrive at the desired set of jump conditions.

$$f_1 = \frac{p - p_0}{\rho_0 a_0^2} + \left(\frac{\rho_0}{\tilde{\rho}} - 1 \right) M^2 + \frac{\rho_s \rho_n w^2}{\rho_0 \tilde{\rho} a_0^2} = 0 \tag{1-40}$$

$$f_2 = \frac{\tilde{\mu} - \mu_0}{a_0^2} + \frac{1}{2a_0^2} \left(\frac{\rho_0}{\tilde{\rho}} a_0 M - \frac{\rho_n}{\tilde{\rho}} w \right)^2 - \frac{1}{2} M^2 = 0 \tag{1-41}$$

$$f_S = \left(\frac{\tilde{s}\, T}{s_0 T_0} - 1 \right) M + \frac{\rho_s \tilde{s}\, T w}{\rho_0 s_0 T_0 a_0}$$

$$+ \frac{\rho_n w}{\rho_0 s_0 T_0 a_0} \left(\frac{\rho_0}{\tilde{\rho}} a_0 M + \frac{\rho_s}{\tilde{\rho}} w \right)^2 = 0 \qquad (1\text{-}42)$$

The wave speed $c = u_0$ has been expressed as the product of a shock Mach number M and a generic upstream sound speed a_0. Generic because shock waves in helium II are of two types which correspond to the linear wave modes of first and second sound in the limit of vanishingly small wave strengths. Thus the Mach number for a pressure (or first sound) shock which primarily jumps the pressure, density, and total flow velocity u is based on first sound speed a_1 while the Mach number for a temperature (or second sound) shock which primarily jumps the temperature, entropy, and counterflow velocity w is based on the second sound speed a_2. For a given upstream thermodynamic state (specified by p_0 and T_0) and a given wave speed $c = Ma_0$, the three jump conditions (1-40) through (1-42), supplemented by state equations for $\tilde{\mu}$, $\tilde{s}$, $\tilde{\rho}$, and $\frac{\rho_n}{\rho}$, specify the downstream state p, T, and w.

1.5. Previous Experimental Work

As an experimental tool, shock waves offer a number of attractive advantages. They impulsively create a well defined flow state in a deterministic way since the amplitudes of jumps across the shock are uniquely related to the wave speed. Wave speeds are precisely measurable and desired values may be generated in ways which repeat reliably. Additionally, shock waves create flow states in the bulk liquid, allowing bulk behavior to be studied in isolation from the complication of boundary effects.

Historically, temperature shocks in helium II were the first type to be investigated. Osborne (1951) generated these by delivering a D.C. pulse to a fine wire. Input powers ranged up to 3.6 W/cm^2. A phosphor bronze resistance thermometer was used to detect the resulting signal which was observed to arrive more quickly as power input was increased. At temperatures close to the lambda transition, the pulse was steepened on the back. At lower temperatures it was front steepened. Dessler and Fairbank (1956) using input powers up to 1.6 W/cm^2 measured the amplitude dependence of second sound signals in liquid helium between 0.936 ^{0}K and 2.045 ^{0}K. Within experimental error their results verified an approximate analytical solution to the jump conditions obtained by Khalatnikov (1952,1965). This approximation (the so called second order theory) will be discussed in the next chapter. Temperature shocks were observed optically by Gulyaev (1967,1970) using Schlieren photography. The experiments were performed at saturated vapor pressure. For heater powers on the order of 3 to 8 W/cm^2, Gulyaev concluded that boiling was seen at the heater surface. The observations of Osborne and Gulyaev were extended quantitatively by Cummings, Schmidt, and Wagner (1978) who used superconducting thin film sensors to measure temperature shock speeds as a function of input heater power and pulse width for various bath temperatures on the saturated vapor pressure curve. They observed deviations from the Khalatnikov second order theory at powers exceeding 5 W/cm^2. Turner (1979) used the same type of sensor to obtain temperature jump measurements across temperature shock waves as a function of their wave speed. A departure from second order theory was observed at roughly $M \geq 1.04$. Counterflow velocities of up to 3.67 m/sec at $T = 1.45$ ^{0}K were generated by temperature shocks in Turner's experiments. This represents the highest w ever attained outside of restricted geometries.

Cummings (1973,1976) simultaneously generated first and second sound shocks in helium II by reflecting a gasdynamic shock from the saturated liquid-

vapor interface. Carbon detectors were used in the gas and the liquid to measure arrival times. Qualitative agreement with the Khalatnikov approximations was observed. The measurements of Cummings were refined and extended by Wise (1979) who used superconducting thin films in addition to carbon detectors to more accurately measure wave speeds in the liquid and vapor phases. For strong pressure shocks in the liquid, Wise observed systematic deviations from the Khalatnikov approximation.

Chapter 2

SOLUTIONS OF THE JUMP CONDITIONS

2.1. The Khalatnikov Approximations

As mentioned previously, whether or not the experimental shock wave data confirm the validity of Landau's equations requires comparison to solutions of the jump conditions which follow from those equations. The solutions against which authors have traditionally compared their results are actually approximations made by Khalatnikov (1952,1965) to the exact solutions. These solutions are approximate in the sense that weak shock waves (i.e., $M = 1 + \varepsilon$) are considered, in which case the jumps in all quantities across the shocks are small. Jumps in temperature $\Delta T = T - T_0$, pressure $\Delta p = p - p_0$, and counterflow velocity w are chosen as the independent variables and each one is considered $O(\varepsilon)$. Then all quantities which appear in the jump conditions (equations (1-40) through (1-42)) are expanded as Taylor series in these variables, and only terms through $O(\varepsilon^2)$ are retained. As a further approximation, the coefficient of thermal expansion is neglected ($\beta \approx 0$). The results for pressure shocks are

$$\Delta p = \frac{2(M-1)}{\left[\frac{\partial}{\partial p} \ln \rho a_1\right]_0} \tag{2-1a}$$

$$\Delta T = 0 \tag{2-1b}$$

$$w = 0 \tag{2-1c}$$

while for temperature shocks Khalatnikov finds

$$\Delta T = \frac{2(M-1)}{\left[\frac{\partial}{\partial T}\ln\frac{a_2^s c_p}{T}\right]_0} \tag{2-2a}$$

$$w = -\left[\frac{\rho s}{\rho_n a_2}\right]_0 \Delta T \tag{2-2b}$$

$$\Delta p = -\left[\frac{\rho_s \rho_n}{\rho} - \frac{\rho^2 a_2^2}{2}\frac{\partial}{\partial p}\left(\frac{\rho_n}{\rho}\right)\right]_0 w^2 \tag{2-2c}$$

Here, as in equations (1-40) through (1-42), the coordinate system is shock-fixed, and the zero subscript refers to the unshocked fluid. The denominator on the right hand side of equation (2-1a) is always positive which means that only compression shocks are to be expected in helium II. High density regions in a propagating pressure disturbance will therefore travel faster than those of low density as was mentioned at the beginning of section 1.4. However the denominator on the right hand side of equation (2-2a) can be either positive or negative depending on the location on the p-T diagram. On the saturated vapor pressure curve it is positive for $T < 0.5\ ^0K$ and for $0.95\ ^0K < T < 1.88\ ^0K$ which means that temperature raising shocks are formed within these regions. Outside of these regions temperature lowering shocks are observed.

2.2. Numerical Solutions

Although the Khalatnikov approximations provide valuable insight into what types of shocks may be observed in helium II, the limitations of their applicability and validity should be borne in mind. First of all they were developed for weak shocks – only terms through second order were retained. Secondly, it is not clear without examining thermodynamic data for helium II whether or not neglecting the coefficient of thermal expansion is consistent with this second order approximation. Owing to the complexity of the jump conditions, for any more exact solutions one must resort to numerical methods. But even numerical solutions cannot be considered to be arbitrarily precise for their quality depends directly on the quality of available experimental thermodynamic data which provide the necessary state equations in a tabular fashion. In fact, the best helium II data to date (Maynard, 1976) provide dependence of the state variables (entropy, density, normal fluid fraction, etc.) on pressure and temperature only. Dependence on counterflow velocity still must be approximated to leading order (w^2) by equations (1-23) through (1-25). The solutions in this thesis should therefore not be taken as "the last word" but only as the best possible given the limitations of current thermodynamic data.

2.2.1. *Solution Method.* Newton's method in three variables may be used to numerically solve the non-linear jump conditions as follows. For a fixed upstream pressure p_0 and temperature T_0 ($w_0 = 0$ always) we seek solution vectors

$$\vec{x} = (p, T, w) \tag{2-3}$$

for the system

$$\vec{f}(\vec{x};M) = 0 \tag{2-4}$$

where

$$\vec{f} = (f_1, f_2, f_3) \tag{2-5}$$

is given by equations (1-40) through (1-42). The shock Mach number M is taken as the independent parameter and is referenced to either the first or second sound speed for pressure or temperature shocks respectively. For M slightly greater than unity, the Khalatnikov approximations would be expected to give a good first guess $\vec{x}_0$. A better solution is then found by Newton's method. (See for example, Isaacson & Keller.)

$$\vec{x}_1 = \vec{x}_0 - J_0^{-1}\,\vec{f}_0 \tag{2-6}$$

J_0^{-1} represents the inverse of the Jacobian at the zeroth value.

$$J_0 = \left[\frac{\partial \vec{f}}{\partial \vec{x}}\right]_0 \tag{2-7}$$

Iterations continue

$$\vec{x}_{\nu+1} = \vec{x}_\nu - J_\nu^{-1}\vec{f}_\nu \tag{2-8}$$

until each f_i approaches zero to within a specified tolerance. At higher Mach numbers, the Khalatnikov solution may be such a poor guess that at best a large number of iterations are required for convergence or at worst no convergence at all is obtained. In such cases, the previous solution $\vec{x}^a$ at Mach number M^a

may be extrapolated in M and used as the initial guess $\vec{x}_0^{\,a+1}$ for the current Mach number M^{a+1}. This is effected by letting

$$\vec{x}_0^{\,a+1} = \vec{x}^{\,a} + \left[\frac{\partial \vec{x}}{\partial M}\right]^a \left(M^{a+1} - M^a\right) \tag{2-9}$$

where

$$\left[\frac{\partial \vec{x}}{\partial M}\right]^a = \left[\left[\frac{\partial \vec{f}}{\partial \vec{x}}\right]^a\right]^{-1} \left[\frac{\partial \vec{f}}{\partial M}\right]^a = \left[J^a\right]^{-1} \left[\frac{\partial \vec{f}}{\partial M}\right]^a \tag{2-10}$$

If the solution vector $\vec{x}$ changes rapidly with M, the Mach number increment on the right hand side of equation (2-9) may be made very small to improve the quality of $\vec{x}_0^{\,a+1}$.

2.2.2. *Previous Implementation.* Sturtevant (1976) used the above approach to solve the jump conditions. Tabular thermodynamic data from a variety of sources existing at that time were used to provide state information. All partial derivatives of the equations $\vec{f}$ with respect to $\vec{x}$ and M were computed numerically by fitting a cubic polynomial through four points which bracketed the current solution point $(\vec{x}, M)$. The fitted polynomial was then differentiated. At each point, the thermodynamic data tables were quadratically interpolated to give the density, entropy, chemical potential, and normal fluid fraction at that point. Due to internal inconsistencies within the thermodynamic data and lack of precision resulting from tabular interpolation, several problems arose. In many cases the numerical solutions did not approach the Khalatnikov approximations as $M \to 1$. In fact, weak wave solutions were often non-convergent. Another problem caused by the data was difficulty in getting back on to the p-T diagram if the result of an iteration landed outside of one of the phase

boundaries. Additionally, the second law of thermodynamics appeared to be violated in some temperature shock cases.

2.2.3. *Current Implementation.* The problems discussed above were eliminated by using the thermodynamic data of Maynard (1976). These data show a high degree of internal consistency since all quantities are constructed from accurate sound speed measurements. Although Maynard tabulates all thermodynamic variables as functions of pressure p, and temperature T, it was determined that interpolation and numerical differentiation of these tables provided insufficient precision to produce reliable weak wave solutions. Thus the actual code which generated the tables (excepting chemical potential) was incorporated into the program (Baker, 1982). Construction of the chemical potential required a somewhat different approach than the other thermodynamic quantities, and the details are given in Appendix A. Within the thermodynamic code, Maynard calculates all pressure and temperature partial derivatives using a single increment of 10^{-4} bar and 10^{-5} ^{0}K respectively. With derivatives taken on this grain, the computer generated values for sound speeds match the experimental data points. For this reason, pressure and temperature partial derivatives within the present shock program were taken in the same way. However, since there are no corresponding natural increment sizes for counterflow velocity w or Mach number M, those partials were computed using the analytical expressions for the derivatives.

Chapter 3

RESULTS

Calculations for shock waves of both the pressure and temperature type were made for a number of upstream pressures p_0 and temperatures T_0 covering the helium II p-T diagram. (See table 3-1.)

Table 3-1. Upstream States

Shock Type	p_0(bar)	T_0(K)			
pressure	SVP	1.30	1.60	1.80	2.10
temperature	1.00	1.30	1.60	1.81	2.10
both	5.00	1.30	1.50	1.70	2.00
both	10.00	1.30	1.50	1.70	1.90
both	15.00	1.30	1.50	1.70	1.90
both	20.00	1.30	1.50	1.80	-

SVP = saturated vapor pressure

For each of these 38 cases (i.e., wave type, p_0, and T_0), shock induced flow states were calculated using upstream Mach number as the independent parameter. Ten plots were generated for each case with the following notation.

1. Trajectories (final states on the helium II p-T diagram) are

indicated by open circles for the numerical solution, and by small dots for the Khalatnikov approximation.

2. The shock Hugoniot (locus of final states on the p-v diagram) is plotted as a solid line for the numerical solution while the Khalatnikov approximation is indicated by a cross symbol. Pressure change divided by upstream pressure ($\Delta p / p_0$) is plotted on the vertical axis and specific volume change over upstream specific volume ($\Delta v / v_0$) is plotted on the horizontal axis.

The remaining eight plots show variation of downstream flow state variables with upstream Mach number, M. In all plots of this type, the numerical solution is shown as a solid line and the Khalatnikov solution as a dashed line. The variables plotted vs. M are:

3. pressure jump, $\Delta p / p_0$
4. temperature jump, $\Delta T / T_0$
5. downstream flow velocity divided by downstream generic sound speed, u / a
6. downstream counterflow velocity divided by downstream generic sound speed, w / a
7. entropy jump, $\Delta s / s_0$
8. entropy flux jump, $\Delta ss / ss_0$
9. downstream normal fluid fraction, ρ_n / ρ
10. heat flux jump, $\Delta q / q_0$

3.1. Representative Pressure Shock Results

Figures 3-1a through 3-1j show the results for pressure shocks with upstream state set at $T_0 = 1.80°K$ and $p_0 =$ saturated vapor pressure.

Figure 3-1a shows the pressure changes, $\Delta p / p_0$ versus Mach number, M for this case. The numerical solution and Khalatnikov approximation coincide as

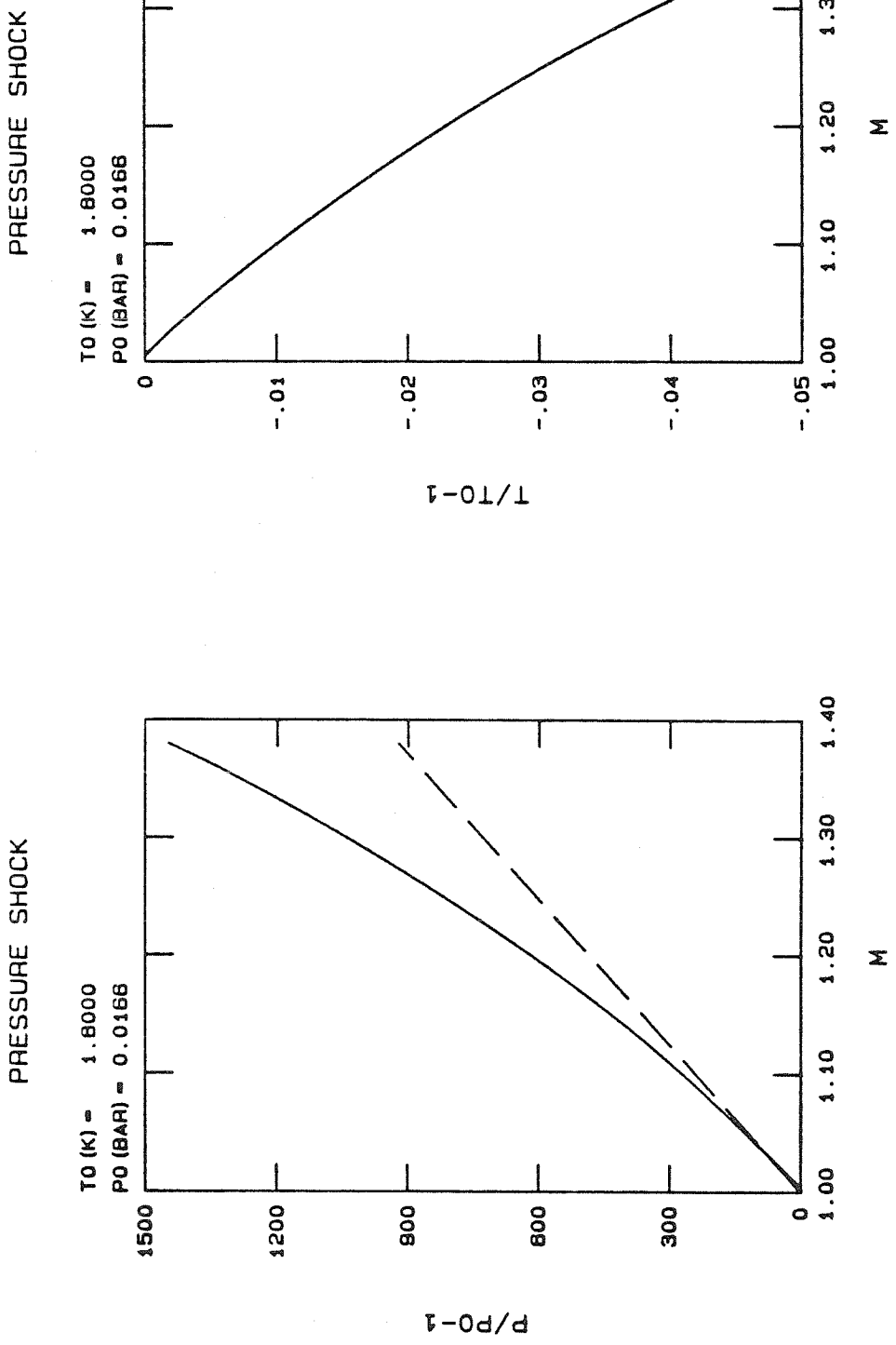

Figure 3-1a. $\frac{\Delta p}{p_0}$ vs. M

Figure 3-1b. $\frac{\Delta T}{T_0}$ vs. M

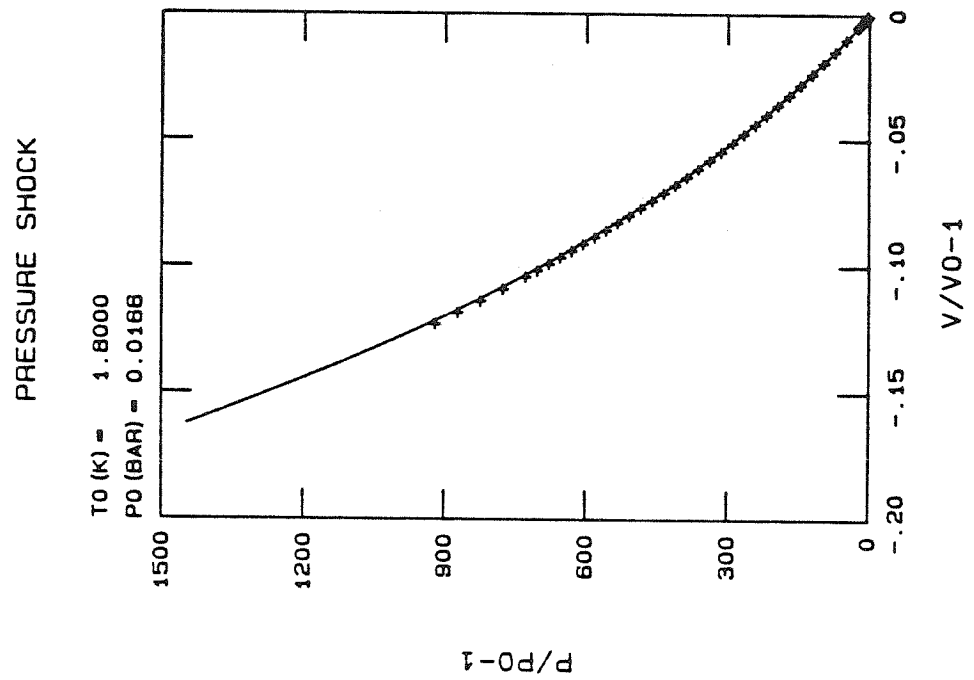

Figure 3-1d. Hugoniot

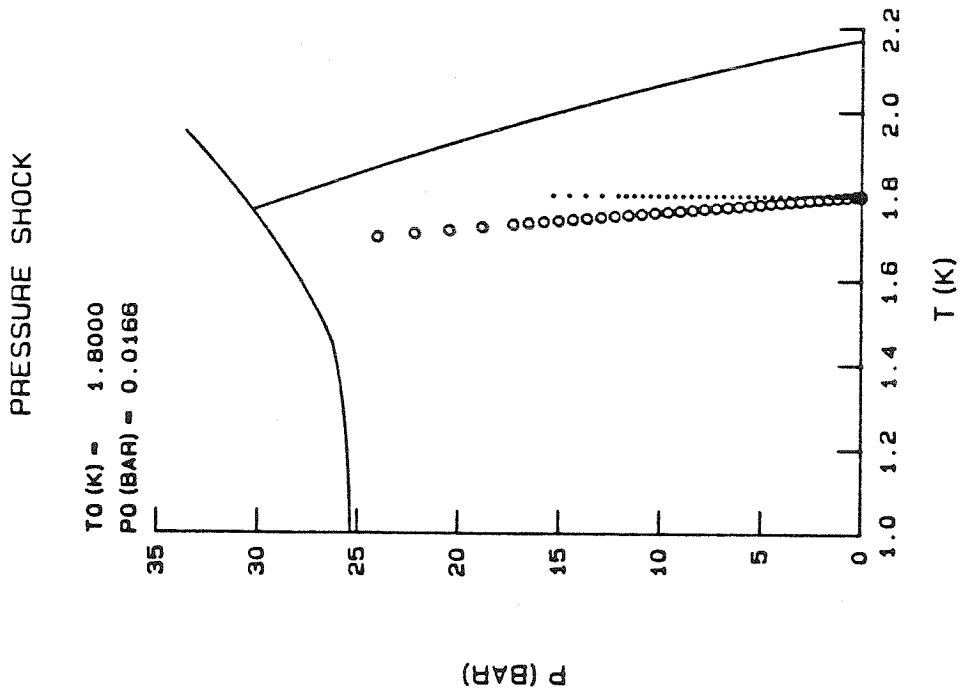

Figure 3-1c. Trajectories

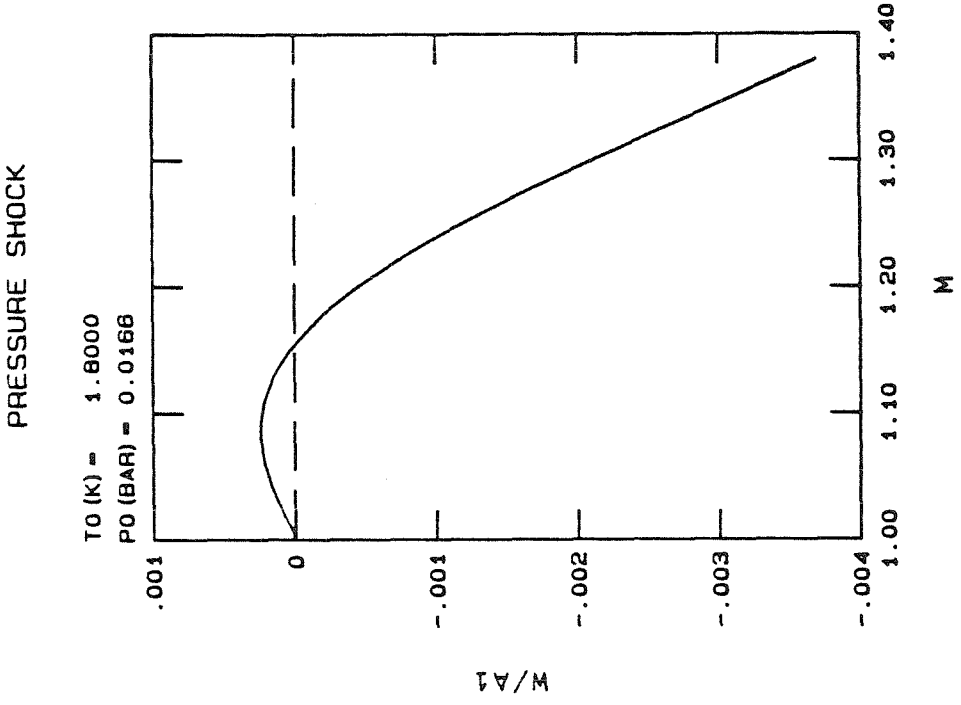

Figure 3-1f. $\frac{w}{a_1}$ vs. M

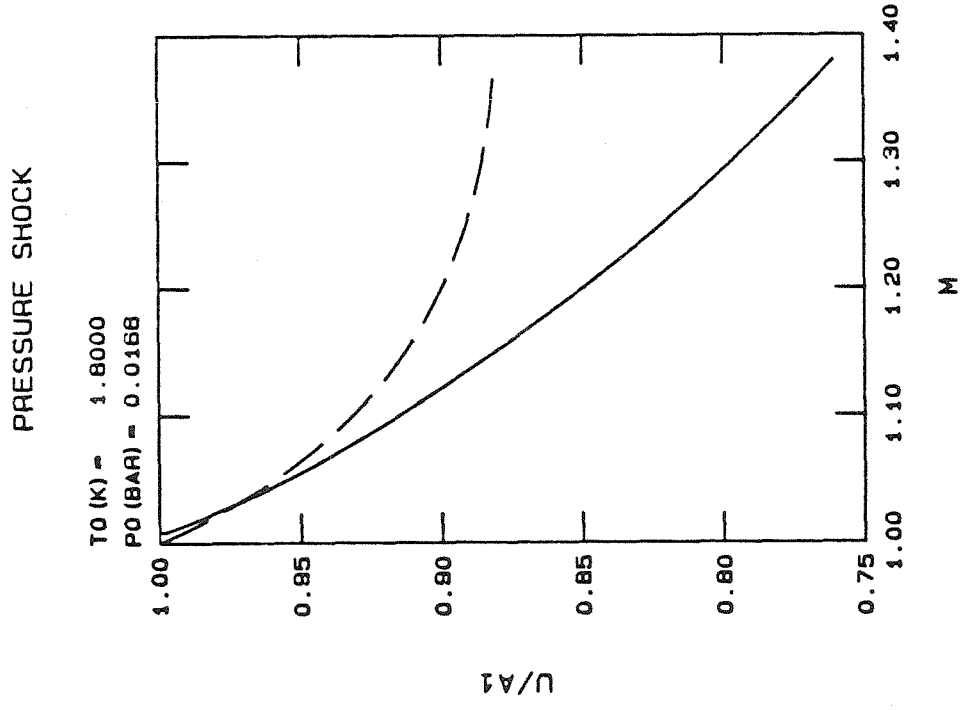

Figure 3-1e. $\frac{u}{a_1}$ vs. M

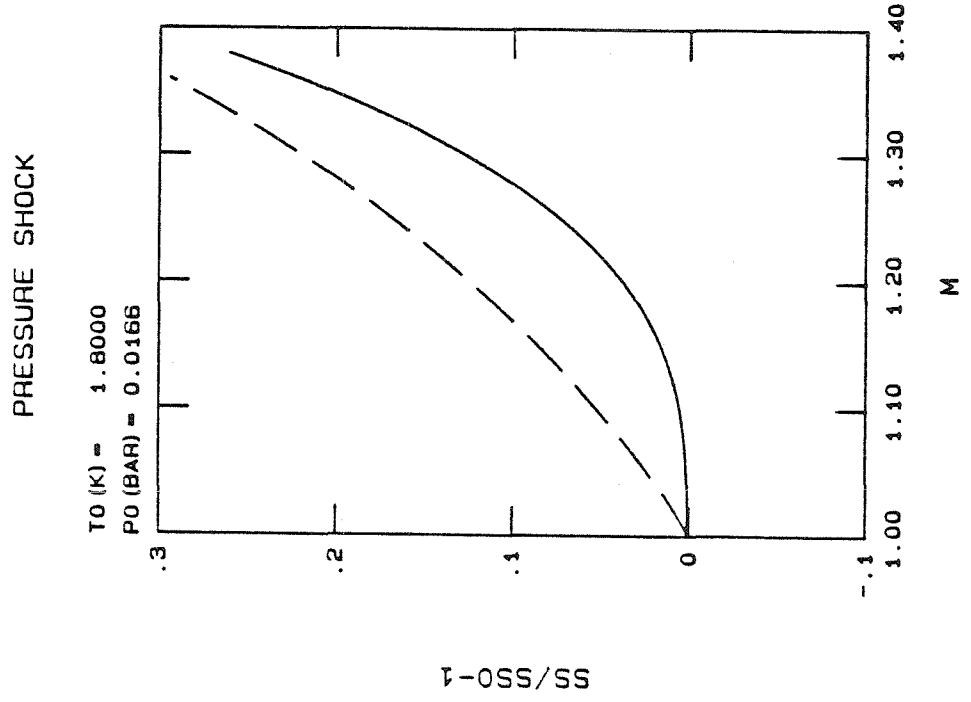

Figure 3-1h. $\frac{\Delta ss}{ss_0}$ vs. M

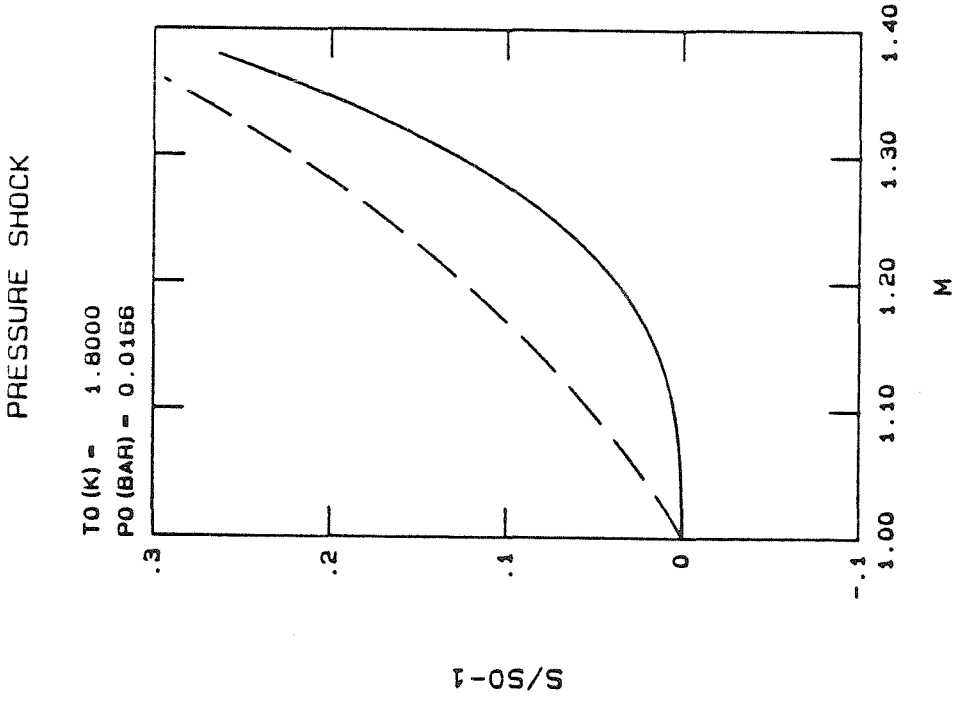

Figure 3-1g. $\frac{\Delta s}{s_0}$ vs. M

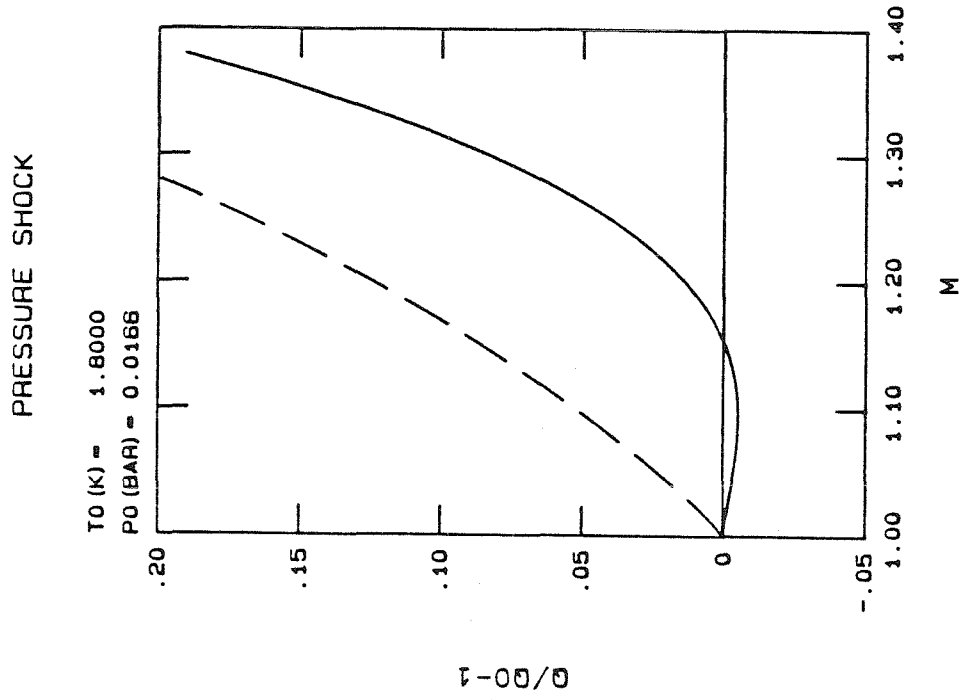

Figure 3-1j. $\frac{\Delta q}{q_0}$ vs. M

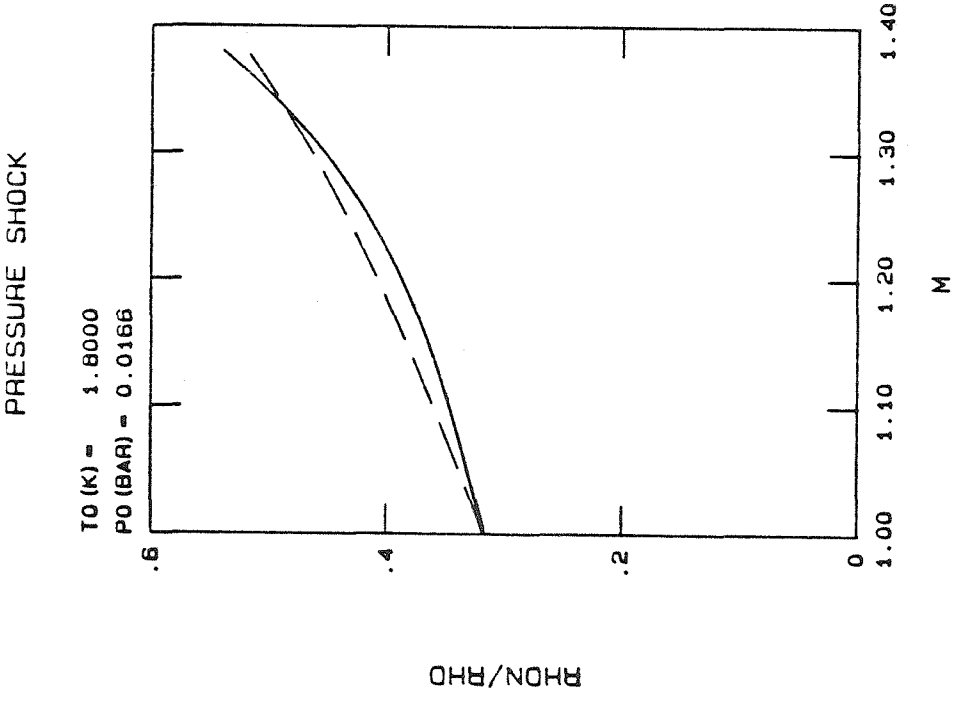

Figure 3-1i. $\frac{\rho_n}{\tilde{\rho}}$ vs. M

they should as $M \to 1$, but for higher Mach numbers the Khalatnikov approximation underestimates the numerically calculated pressure jump. These same qualitative features in $\Delta p/p_0$ vs. M are seen in the 18 other pressure shock cases as well.

Figure 3-1b shows the changes in temperature ($\Delta T/T_0$ *vs.* M) for this case. While Khalatnikov approximates pressure shocks in helium II as isothermal processes, the full numerical solution indicates a temperature decrease, the magnitude of which increases as the wave strength increases. This trend of continuously larger temperature decreases is not always seen. For example, for the pressure shock case having upstream conditions set on the SVP curve at $T_0 = 1.30°K$, the temperature change is initially a decrease for low Mach numbers, but for M greater than 1.13, ΔT across the shock becomes positive.

Trajectories for the representative case are shown in Figure 3-1c. The highest pressure final state for the numerical solution corresponds to $M = 1.38$. For $M = 1.39$, the numerical solution for downstream pressure is above 25 bar which is outside the range of Maynard's thermodynamics. The Hugoniot shown in Figure 3-1d is of the type most frequently seen in gasdynamics. The slope is negative which is the only possibility in a classical material while the curvature is positive, indicating occurrence of compression shocks.

Figures 3-1e and 3-1f show respectively the flow and counterflow velocities behind the shock divided by downstream first sound speed. Since the flow is compressed through the shock to a higher density, the downstream flow velocity u jumps to ever lower (increasingly subsonic) values as the upstream Mach number increases. The same result is also observed for classical shocks where u is the only flow velocity. For the counterflow velocity w produced by the pressure shock, we see an interesting behavior. Within Khalatnikov's approximations, a pressure shock induces zero w. The full numerical solution shows that

in this representative case, w is initially positive (away from the shock), goes through zero at $M = 1.16$ and becomes increasingly negative (toward the shock) for higher Mach numbers. This is more or less a general trend for all the pressure shock cases which were computed although the Mach number at which w passes through zero increases as the initial temperature T_0 increases on any given initial isobar. For those pressure shock cases close to the lambda line, w is always positive since before higher Mach numbers can be attained, the final state has crossed the lambda line.

In discussing entropy change across a superfluid shock wave, account must be taken of the transport of heat by convection with the normal fluid velocity. For any general fluid flow through some fixed control volume V, the second law of thermodynamics can be expressed as a nonconservation equation.

$$\frac{d}{dt}\int_V \rho s \, dV \geq -\int_A \frac{\vec{q}}{T}\cdot d\vec{A} \tag{3-1}$$

Here A is used for the closed surface bounding V, and the surface element normal vector is taken positive outward as is customary. The heat flux vector at the boundary is denoted by $\vec{q}$ and hence $\frac{\vec{q}}{T}$ represents the entropy flux. In words, expression (3-1) states that the rate of entropy increase in V exceeds or equals the entropy flux into V. Since all entropy in helium II resides in the normal fluid fraction, heat flux in this liquid is given by (see Landau & Lifshitz, 1959)

$$\vec{q} = \tilde{\rho}\tilde{s}\,T\,\vec{u}_n \tag{3-2}$$

Applying equation (3-1) to the steady, one-dimensional flow through a fixed

superfluid shock gives the following:

$$\frac{q}{T} - \frac{q_0}{T_0} \geq 0 \tag{3-3a}$$

or, denoting entropy flux by ss

$$\Delta ss \geq 0 \tag{3-3b}$$

or, using equation (3-2) for $\vec{q}$

$$\tilde{\rho}\,\tilde{s}\,u_n - \rho_0 s_0 u_{n_0} \geq 0 \ . \tag{3-3c}$$

By using equation (1-15) to replace u_n in favor of u and w, this becomes :

$$\tilde{s}(\tilde{\rho}u + \rho_s w) - s_0 \rho_0 u_0 \geq 0 \tag{3-4}$$

Conservation of mass as expressed by equation (1-36) can be used to write expression (3-4) as

$$\frac{\tilde{s}}{s_0}\left(1 + \frac{\rho_s w}{\rho_0 u_0}\right) - 1 \geq 0 \ . \tag{3-5}$$

Expression (3-5) is a generalization of the gasdynamic axiom: 'Entropy must increase across a shock." This statement is a proper consequence of the second law of thermodynamics for the classical case where $w = 0$. However, due to the presence of reversible, convective heat flux, the statement for helium II should be generalized to: 'Entropy *flux* must increase across a shock." Positive w indicates reversible extraction of heat from the flow behind the shock which results

in the possibility of the entropy itself decreasing. The normalized changes in entropy $\Delta s/s_0$ and entropy flux $\Delta ss/ss_0$ are shown for the representative pressure shock case in figures 3-1g and 3-1h, respectively. Since the counterflow velocity, w, is much smaller than the upstream velocity, u_0, the differences in the two plots are insignificant. Such will not be the case for temperature shocks when $\rho_s w/\rho_0 u_0$ is large. From very general thermodynamic reasoning, the curve for change in entropy flux should have zero slope and curvature as $M \to 1$. That is, the entropy flux change should be of order $(M-1)^3$ for very weak waves. From figure 3-1h, the solid line which represents the numerical solution fulfills these expectations. The plotted Khalatnikov entropy flux change (dashed line) obviously does not. The reason can be seen from examining the energy equation (1-39) rewritten below.

$$\tilde{\rho}\,\tilde{s}\,T\,u_n + \rho_n\,u_n^2 w = \rho_0\,s_0\,T_0\,u_{n_0} \tag{3-6}$$

According to Khalatnikov's approximations for pressure shocks, $T = T_0$ and $w = 0$. Substituting these, together with continuity (1-36), and equation (1-15) for u_n gives simply

$$\tilde{s}(p, T_0, w = 0) = s_0(p_0, T_0) \tag{3-7}$$

Thus the energy equation is satisfied in the Khalatnikov pressure shock approximation only if $\left(\frac{\partial s}{\partial p}\right)_T = 0$. This is equivalent to neglecting the coefficient of thermal expansion β since

$$\beta = -\frac{1}{\rho}\left(\frac{\partial \rho}{\partial T}\right)_p = -\rho\left(\frac{\partial s}{\partial p}\right)_T .$$

As mentioned before, the Khalatnikov formulas for the final state are arrived at by taking $\beta = 0$. However, within the computer program, any final state regardless of whether it is calculated by the Khalatnikov approximation or found iteratively by Newton's method, is used as input to Maynard's thermodynamic subroutines to calculate all additional state variables (entropy, density, normal fluid fraction, etc.). Since β is in fact small and negative but not precisely zero in the true thermodynamics, the dashed lines on plots of secondary quantities (i.e., those which are not given explicitly in the six Khalatnikov equations) can either be disregarded as inconsistent with the Khalatnikov approximation or taken to show the error which results from neglecting the coefficient of thermal expansion. For example, by equation (3-7), the dashed line in Figure 3-1g should be horizontal, but since $\beta < 0$ the entropy will in fact increase with pressure as indicated by the dashed line which is actually plotted.

Figures 3-1i and 3-1j show downstream normal fluid fraction and change in heat flux, respectively. According to equation (3-2), the energy equation (3-6) may be written in terms of the heat flux change across the shock directly.

$$\Delta q = q - q_0 = -\rho_n u_n^2 w \tag{3-8}$$

Thus Δq should be of opposite sign to w. This is the case for the numerically calculated Δq (solid line in Figure 3-1j), but the dashed line is not horizontal even though w by Khalatnikov is zero here. The reason is the same as for the entropy plots, that is, $\beta \neq 0$. In fact, note that since $T = T_0$ by Khalatnikov that this implies $\Delta q / q_0$ and $\Delta ss / ss_0$ are identical. The dashed lines in Figures 3-1h and 3-1j are therefore the same curve.

3.2. Representative Temperature Raising Shock Results

As was discussed in section 2.1, temperature shocks may either be temperature raising or temperature lowering processes depending on the sign of the denominator on the right hand side of equation (2-2a). Figures 3-2a through 3-2j show the calculated results for the temperature shock case with upstream state set at T_0 = 1.60°K and p_0 = 1.00 bar. At this point on the p-T diagram, the above mentioned denominator is positive which means that temperature shocks should process this upstream state to a higher downstream temperature, at least for weak shocks.

Figure 3-2b shows the temperature changes, $\frac{\Delta T}{T_0}$ versus Mach number, M for this case. As with the previously discussed pressure shock case, the numerical solution (solid line) and Khalatnikov approximation (broken line) coincide as $M \rightarrow 1$. However, for higher Mach numbers, the Khalatnikov approximation overestimates the numerically calculated temperature jump. In fact, the numerical solution for $\frac{\Delta T}{T_0}$ is seen to pass through a maximum of $\left(\frac{\Delta T}{T_0}\right)_{max} \approx 0.07$ at $M \approx 1.50$. At Mach numbers higher than 1.50, $\frac{\Delta T}{T_0}$ continuously decreases. These same qualitative features for the numerically calculated temperature jumps are seen in the 13 other temperature raising shock cases as well. The behavior of the $\frac{\Delta T}{T_0}$ vs. M curve for temperature raising shocks varies negligibly as a function of upstream pressure p_0, but it does vary somewhat as a function of upstream temperature, T_0. For example, $\left(\frac{\Delta T}{T_0}\right)_{max} \approx 0.06$ and occurs at $M \approx 1.26$ when T_0 = 1.81°K and p_0 = 1.00 bar.

Figure 3-2a shows the pressure jumps versus Mach number for the representative case. All temperature shocks in helium II, whether temperature raising or

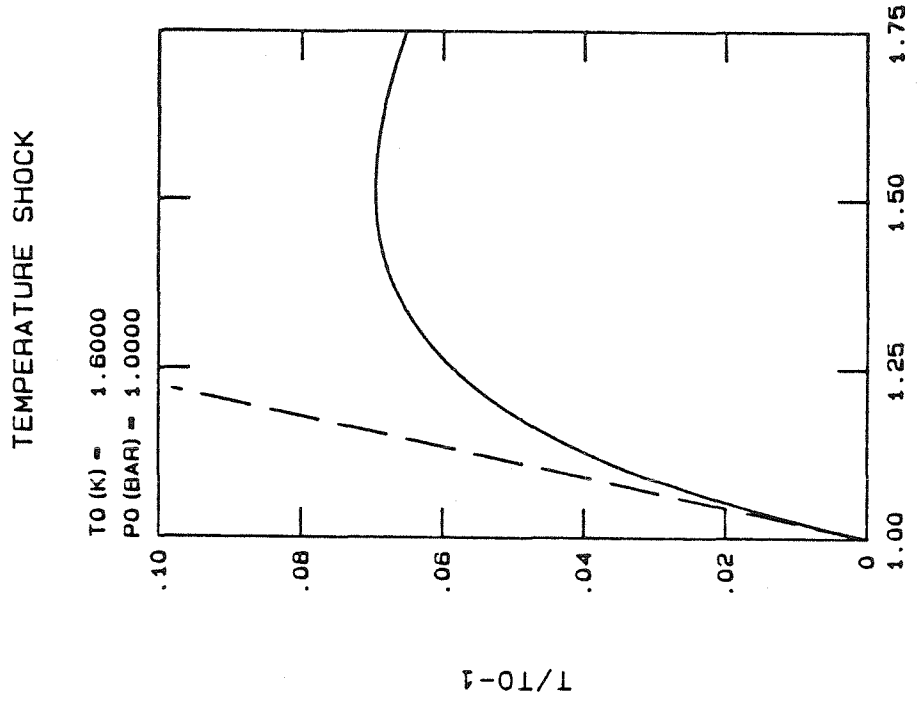

Figure 3-2b. $\frac{\Delta T}{T_0}$ vs. M

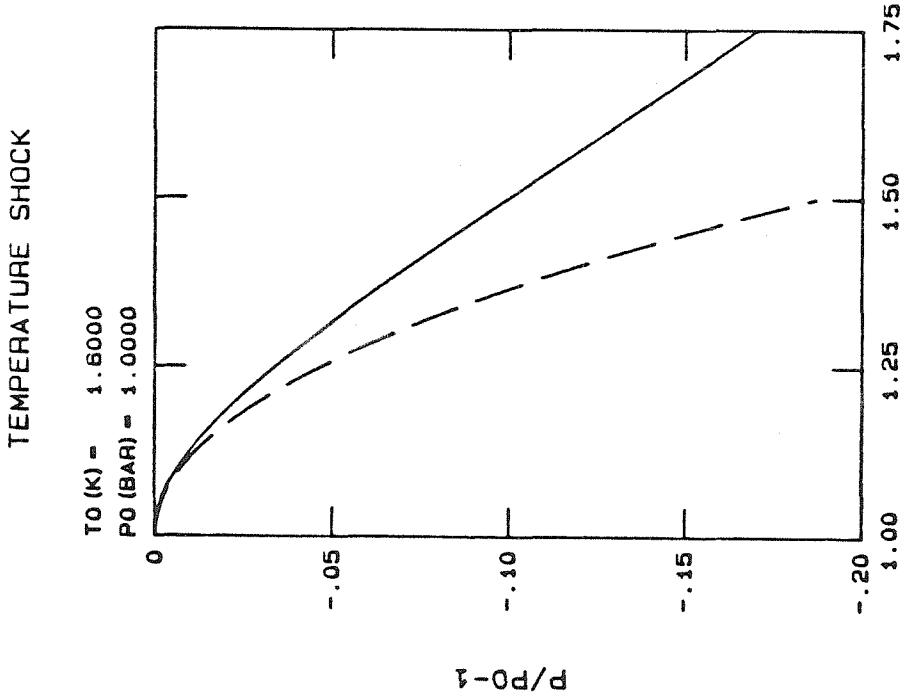

Figure 3-2a. $\frac{\Delta p}{p_0}$ vs. M

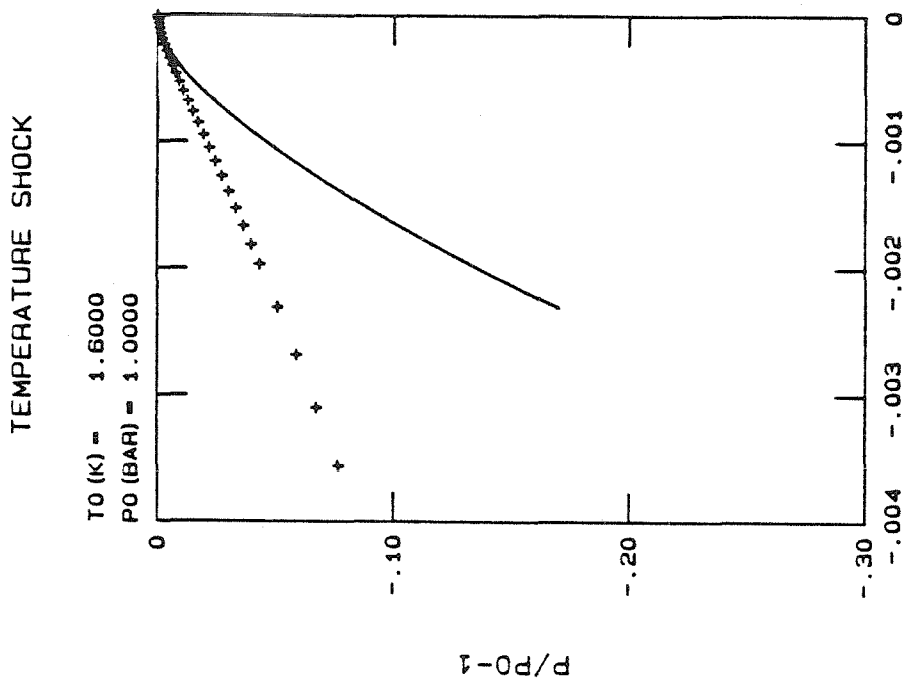

Figure 3-2d. Hugoniot

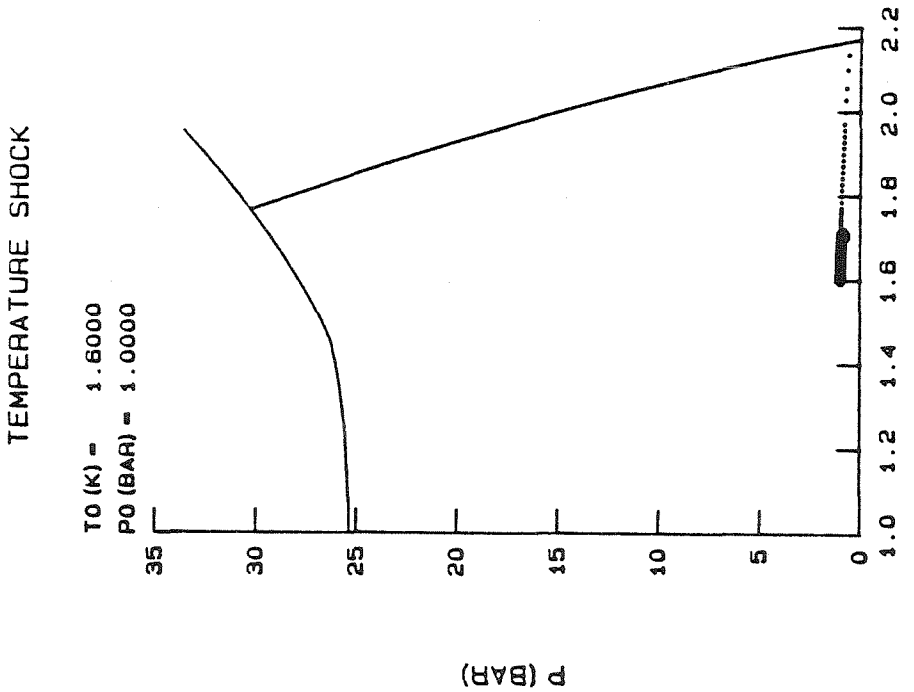

Figure 3-2c. Trajectories

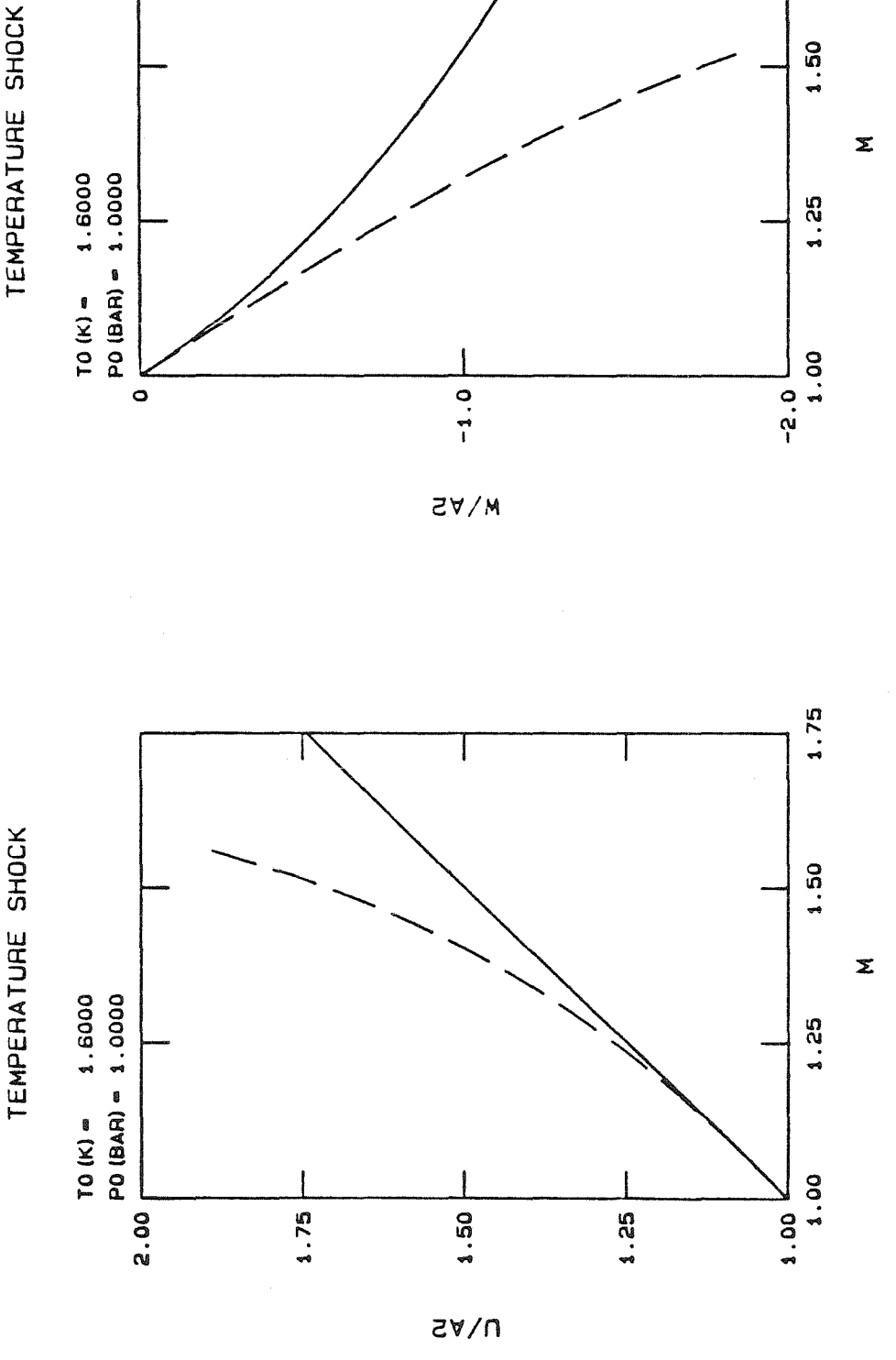

Figure 3-2e. $\frac{u}{a_2}$ vs. M

Figure 3-2f. $\frac{w}{a_2}$ vs. M

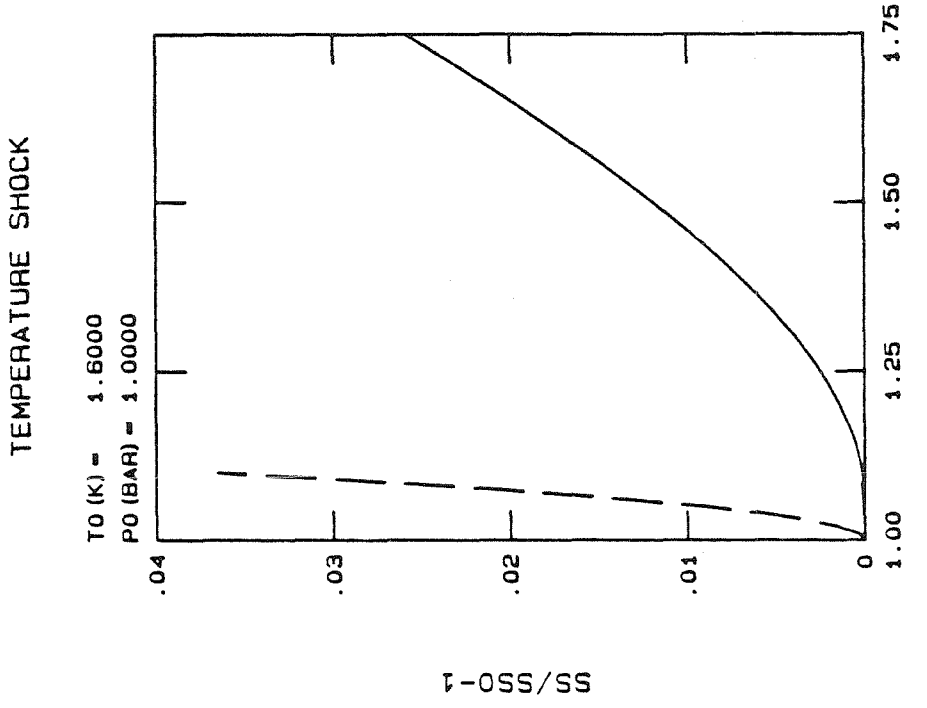

Figure 3-2h. $\frac{\Delta ss}{ss_0}$ vs. M

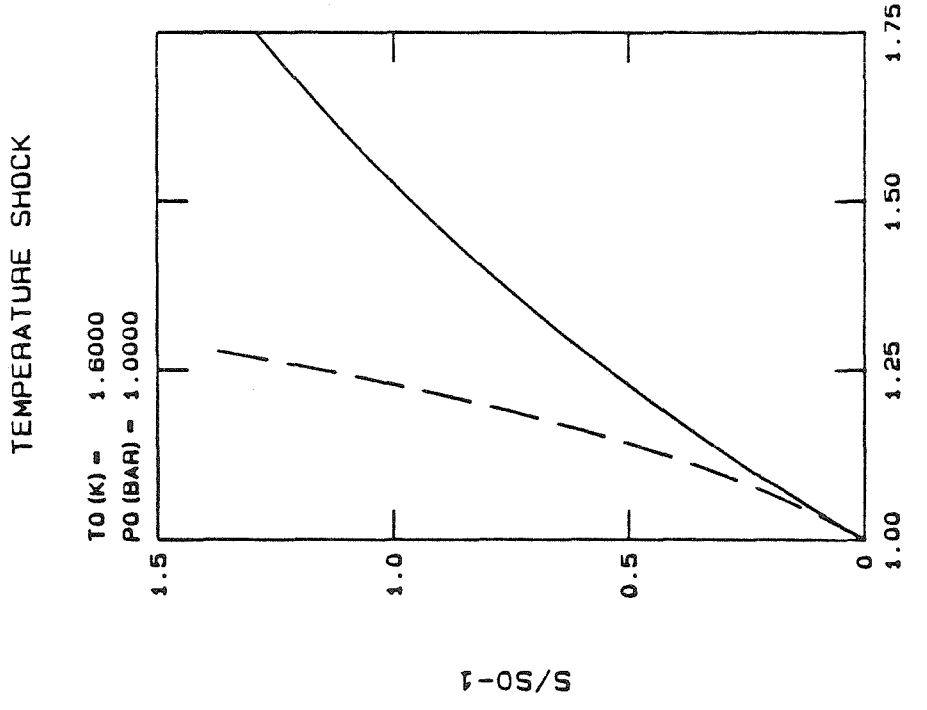

Figure 3-2g. $\frac{\Delta s}{s_0}$ vs. M

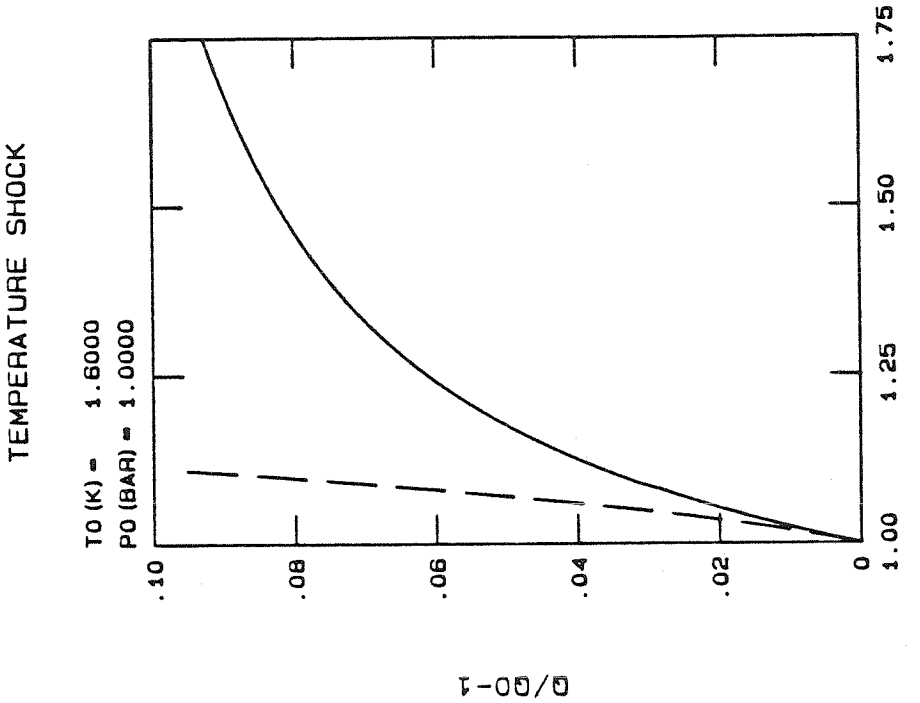

Figure 3-2j. $\frac{\Delta g}{g_0}$ vs. M

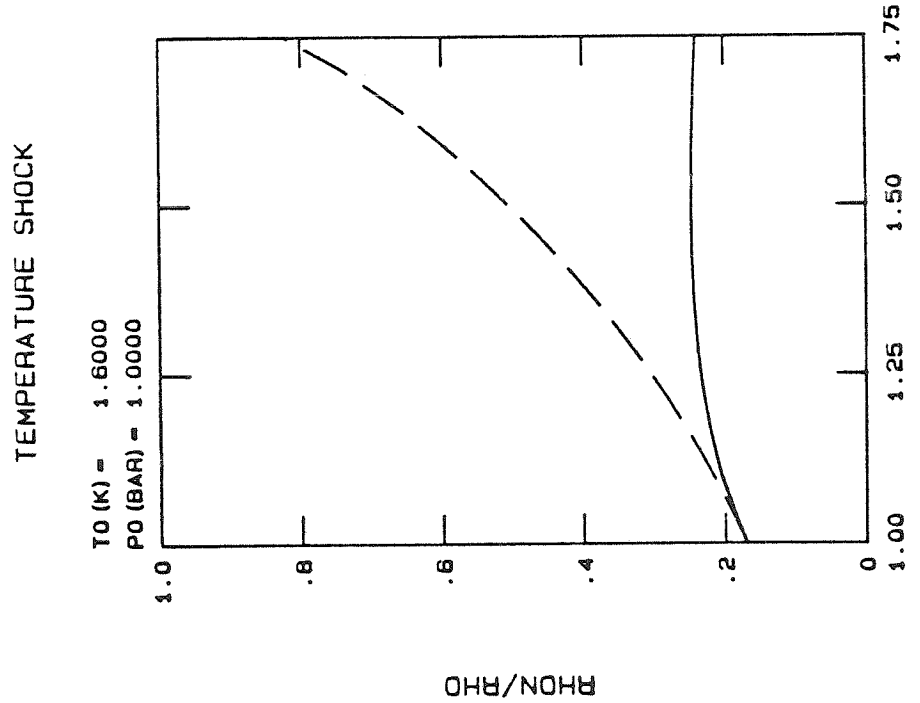

Figure 3-2i. $\frac{\rho_n}{\tilde{\rho}}$ vs. M

temperature lowering, are pressure lowering processes. Corresponding to the smaller magnitude of temperature increase for the numerical solution, the magnitude of the numerical pressure decrease across temperature raising shocks is also seen to be smaller than that approximated by Khalatnikov.

The trajectories for this case are shown in Figure 3-2c. The numerically computed final states which are represented by open circles, lie so close together as to overlap and appear as a short thick solid line. The Khalatnikov final state (small dot) lying closest to the lambda line corresponds to $M = 1.75$. For $M \geq 1.76$, the Khalatnikov final states lie off the helium II p-T diagram for this case.

Figure 3-2d shows the Hugoniot for this case. Remarkably, the Hugoniots for temperature raising shocks have positive slope. The reason can be seen by combining the equations of mass conservation (1-36) and momentum conservation (1-37) which are written below.

$$j = \tilde{\rho} u = \rho_0 u_0 \tag{3-9}$$

$$p + \rho_s u_s^2 + \rho_n u_n^2 = p_0 + \rho_0 u_0^2 \tag{3-10}$$

Upon eliminating u_s and u_n in favor of u and w by equations (1-15) and (1-16) and replacing the density with the specific volume ($\tilde{\rho} = 1 / \tilde{v}$), equations (3-9) and (3-10) may be combined to give

$$\frac{\Delta p}{\Delta v} = -j^2 - \frac{(v_0 + \Delta v)\rho_s \rho_n w^2}{\Delta v} \tag{3-11}$$

For classical fluids, $w = 0$, and the Hugoniot slope given by equation (3-11) is

therefore always negative. For pressure shocks in helium II, $w \approx 0$, and as seen in the previous section, $\frac{\Delta p}{\Delta v}$ will be negative for these cases also. However, for temperature shocks, the mass flux is small, as are the jumps in pressure and density across the shock. Thus, from equation (3-11) we have

$$\frac{\Delta p}{\Delta v} \approx - \frac{v_0 \rho_s \rho_n w^2}{\Delta v} \tag{3-12}$$

Since $\Delta p < 0$ for all temperature shocks, the sign of the Hugoniot slope is determined by the sign of Δv (change in specific volume). Since pressure changes are small, the density (i.e., inverse specific volume) change across temperature shocks is dominated by the temperature change. The negative coefficient of thermal expansion for helium II implies a specific volume decrease upon a temperature increase and visa-versa. Equation (3-12) thus correctly predicts a positive sloping Hugoniot for temperature raising shocks ($\Delta T > 0$) and negative slopes for temperature lowering shocks.

Figures 3-2e and 3-2f show the downstream velocity fields normalized by the downstream second sound speed. For this case, the numerically computed downstream Mach number for flow velocity u/a_2 is virtually equal to the upstream Mach number $M = u_0/a_{2_0}$. The downstream counterflow velocity is seen to be negative (toward the shock) which is an indication of heat addition from the downstream region.

Plots of jumps in entropy and entropy flux for this case are shown in figures 3-2g and 3-2h, respectively. Since the relative velocity w is large for temperature shocks, the two plots are seen to differ substantially as would be expected from equation (3-5).

Downstream normal fluid fraction and heat flux jump are shown in figures 3-2i and 3-2j, respectively. Since the relative velocity is always negative for this case, the heat flux jump is positive as dictated by equation (3-8).

3.3. Representative Temperature Lowering Shock Results

Figures 3-3a through 3-3j show the calculated results for the temperature shock case with upstream state set at $T_0 = 2.10°K$ and $p_0 = 1.00$ bar. At this point on the p-T diagram, temperature shocks are of the temperature lowering variety.

From figure 3-3b, it can be seen that the Khalatnikov approximation underestimates the magnitude of the temperature decrease across stronger shocks and, correspondingly from figure 3-3a the magnitude of the pressure decrease as given by Khalatnikov is also too small when compared to the exact solution.

The trajectories shown on figure 3-3c proceed from right to left as the Mach number increases. The Khalatnikov final states (small dots) are for the most part covered by the open circles representing the numerically calculated final states. The Hugoniot shown in figure 3-3d now has a negative slope since the superfluid volume increases with decreasing temperature.

Figure 3-3e shows that the numerically calculated downstream normalized flow velocity for this case initially decreases to 0.92 at $M = 1.55$ and then begins to increase for higher Mach numbers. As shown in figure 3-3f, the relative velocity is positive (away from the shock) which indicates an extraction of heat from the downstream region

As a consequence of this heat extraction, the entropy change across the shock is negative as can be seen in figure 3-3g. However, the entropy *flux* increases (see figure 3-3h) as it must by the second law of thermodynamics.

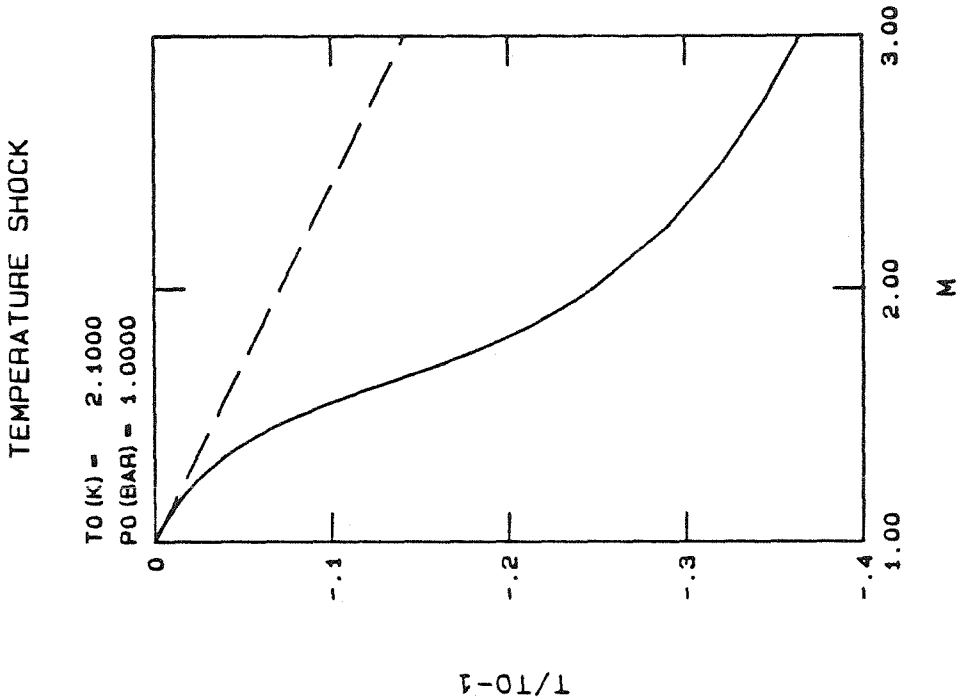

Figure 3-3b. $\frac{\Delta T}{T_0}$ vs. M

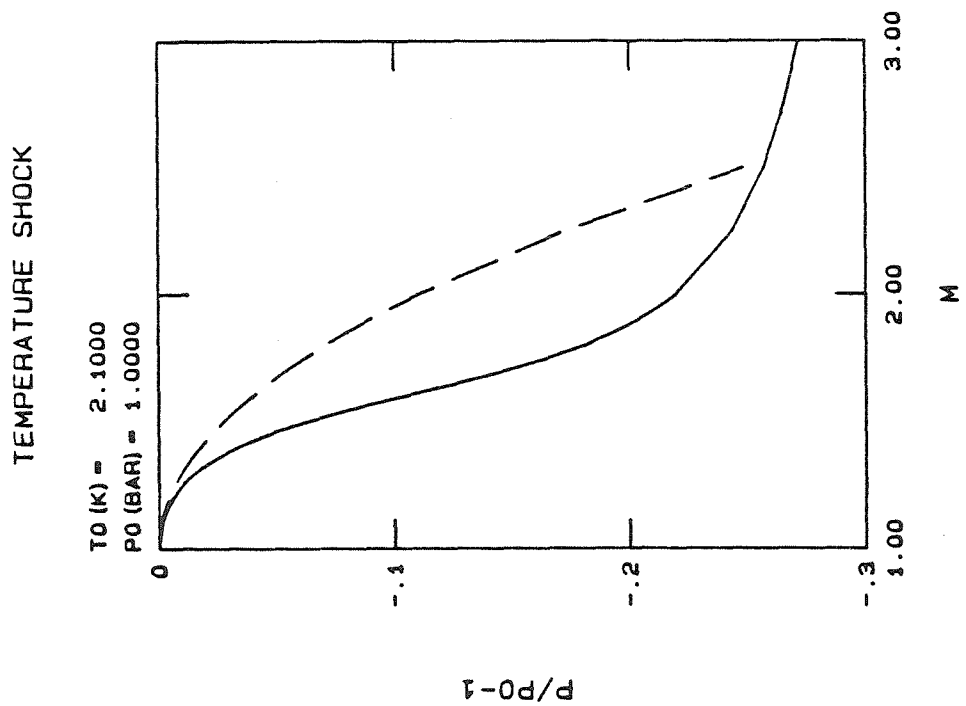

Figure 3-3a. $\frac{\Delta p}{p_0}$ vs. M

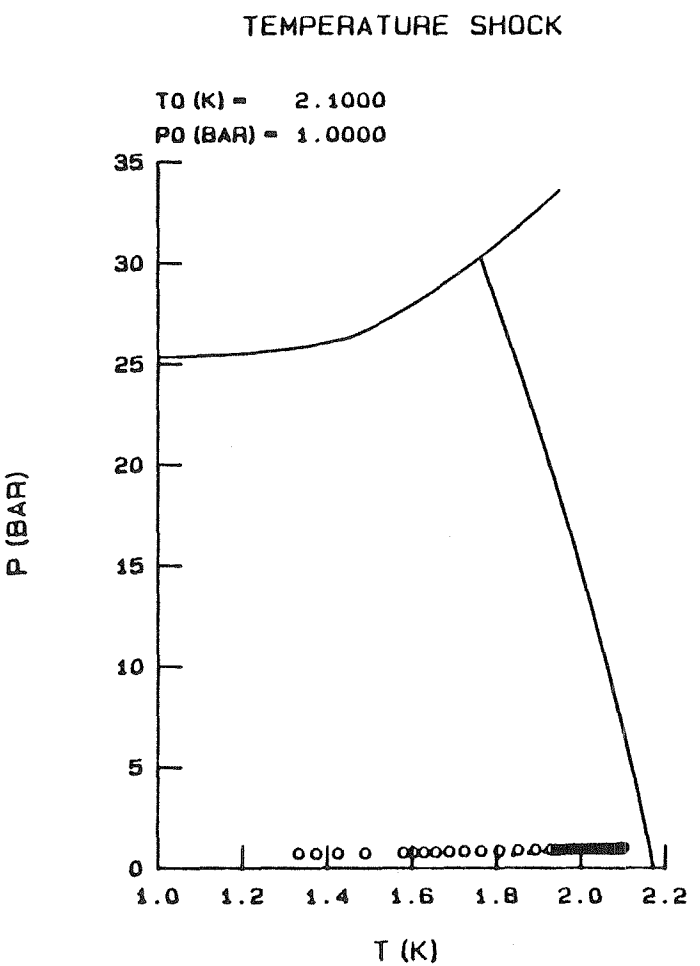

Figure 3-3c. Trajectories

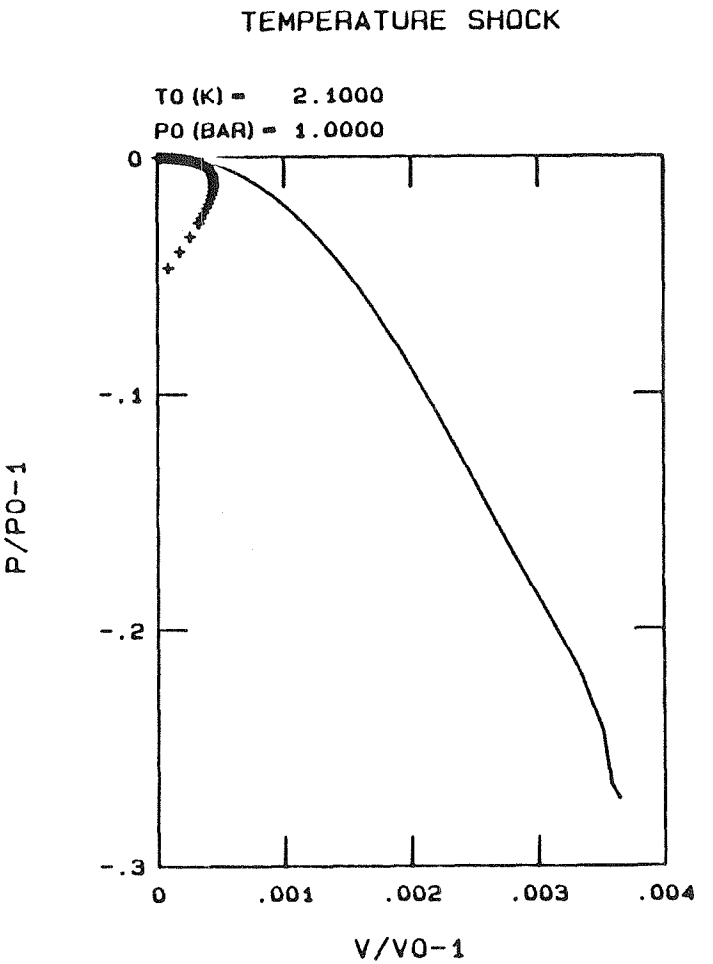

Figure 3-3d. Hugoniot

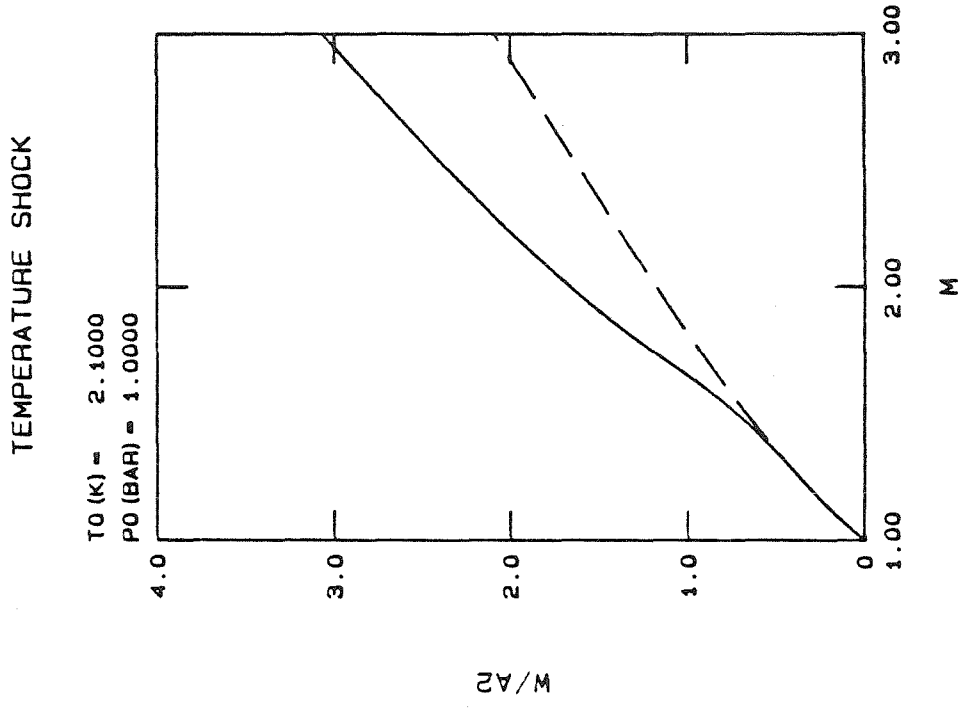

Figure 3-3f. $\frac{w}{a_2}$ vs. M

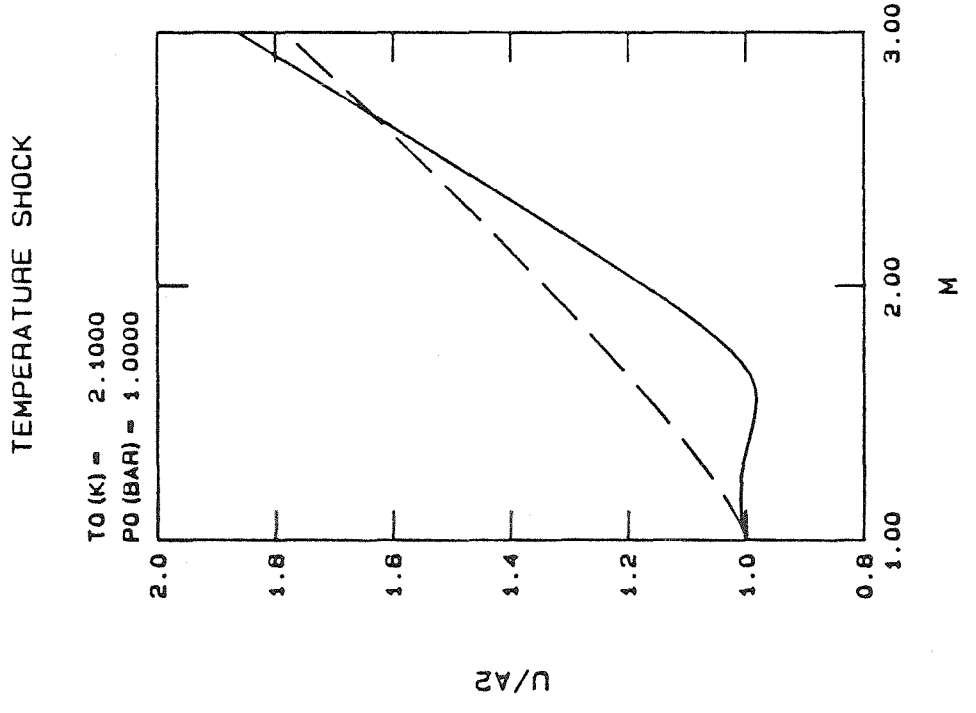

Figure 3-3e. $\frac{u}{a_2}$ vs. M

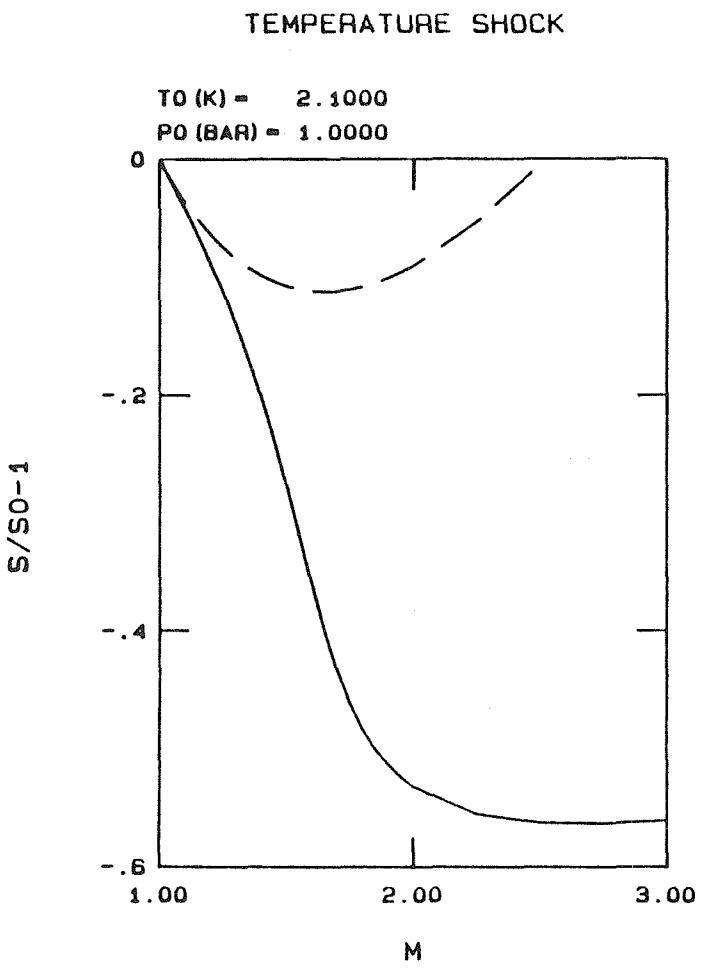

Figure 3-3g. $\frac{\Delta s}{s_0}$ vs. M

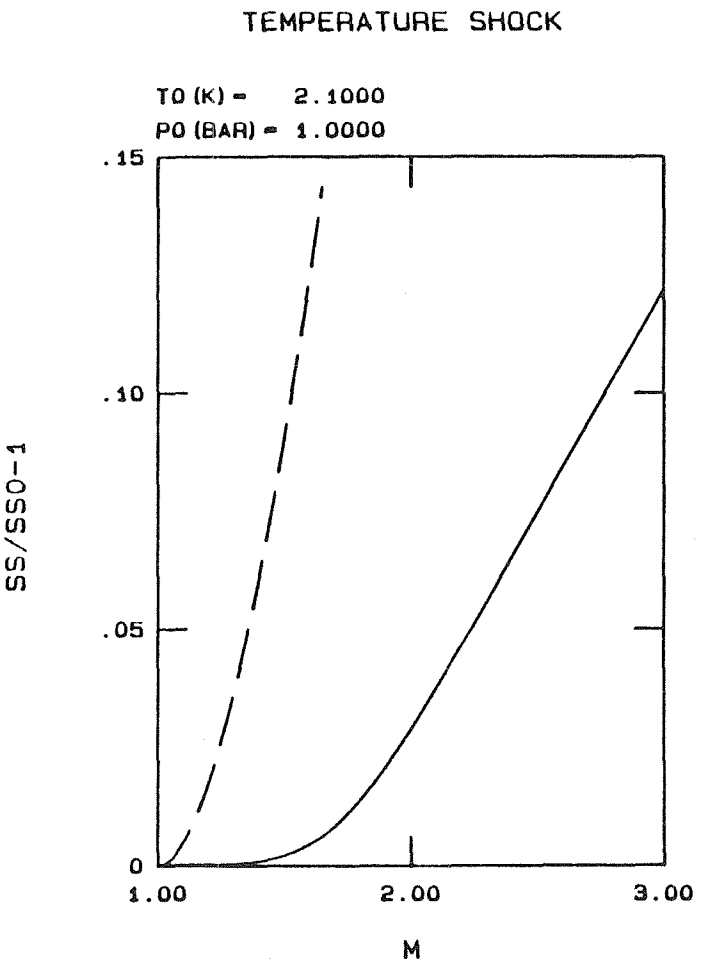

Figure 3-3h. $\frac{\Delta ss}{ss_0}$ vs. M

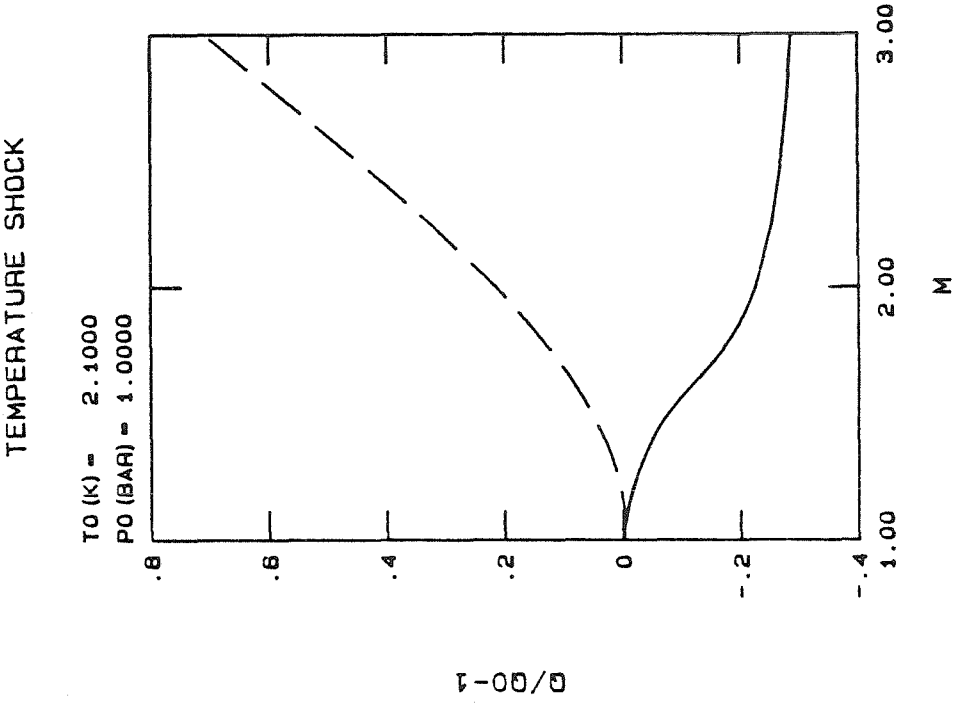

Figure 3-3j. $\frac{\Delta q}{q_0}$ vs. M

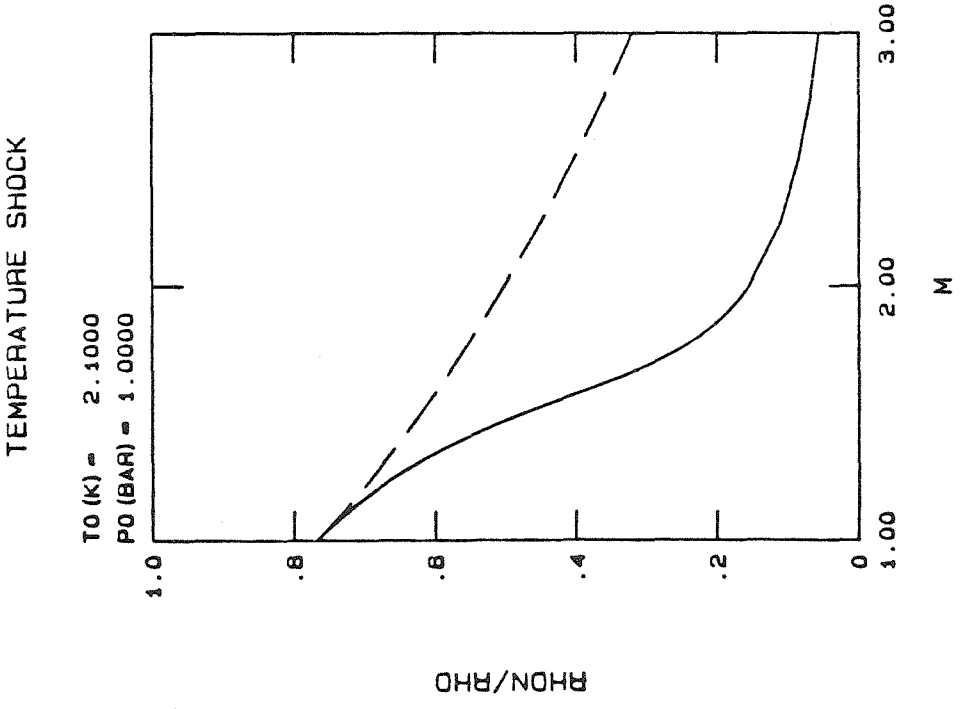

Figure 3-3i. $\frac{\rho_n}{\tilde{\rho}}$ vs. M

(See equation (3-5).)

The numerically calculated heat flux jump shown in figure 3-3j is negative as it should be since w is positive. The heat flux change as calculated from the Khalatnikov final states is initially negative but quickly becomes positive as M increases. This does not represent a violation of energy conservation (equation (3-8)) since as mentioned previously, the Khalatnikov results for such secondary quantities as heat flux may be disregarded since the thermodynamics used to calculate them is inconsistent with the approximation of zero coefficient of thermal expansion.

3.4. Comparison of Numerical and Experimental Results

Data from the experiments of Wise (1979) may be compared to the numerical results for pressure shocks. In these experiments, a first sound shock in the liquid was produced by allowing a gasdynamic shock to reflect from the liquid surface. Starting at seven different temperatures T_0 on the SVP curve, Wise measured velocities of the incident and reflected gasdynamic shocks plus the velocity of the transmitted pressure shock in the liquid.

Using the ideal gas shock jump conditions, with the two measured wave speeds in the helium vapor, one may calculate the pressure jump on the vapor side of the interface $\left[\frac{\Delta p}{p_0}\right]_{GAS}$. Similarly, the wave speed of the pressure shock in the liquid, may be used to calculate the pressure jump on the liquid side of the interface both numerically $\left[\frac{\Delta p}{p_0}\right]_N$ and by Khalatnikov's approximation $\left[\frac{\Delta p}{p_0}\right]_K$. The pressures across the interface should match. Table 3-2 shows these calculations with Mach number for the pressure shock in the liquid given in the rightmost column.

Table 3-2. Pressure Jumps across Pressure Shocks

Exp't	T_0(K)	p_0	$(\Delta p/p_0)_{CAS}$	$(\Delta p/p_0)_N$	$(\Delta p/p_0)_K$	M
a	1.522	SVP	1381.	1332.	1129.	1.145
b	1.665	"	602.7	558.2	489.2	1.119
c	1.751	"	642.9	583.8	479.1	1.164
d	1.832	"	446.0	498.3	400.4	1.184
e	1.989	"	293.9	244.2	208.5	1.161
f	2.031	"	298.9	202.0	176.7	1.155
g	2.095	"	315.7	283.0	226.0	1.241

Table 3-3. Temperature Jumps across Pressure Shocks

Exp't	T_0(K)	p_0	M	$\left[\frac{\Delta T}{T_0}\right]_{EXP}$	$\left[\frac{\Delta T}{T_0}\right]_N$	$(w/a_{1_0})_N$
						$\times 10^4$
a	1.522	SVP	1.145	-.0079	-.0117	-11.3
b	1.665	"	1.119	-.0126	-.0118	-.522
c	1.751	"	1.164	-.0200	-.0180	-2.90
d	1.832	"	1.184	-.0180	-.0212	-1.99
e	1.989	"	1.161	-.0241	-.0191	4.86
f	2.031	"	1.155	-.0291	-.0186	6.07
g	2.095	"	1.241	-.0263	-.0377	8.22

In all seven cases, the numerical result agrees more closely than the Khalatnikov approximation to the pressure jump in the gas. For the first four cases (lower temperatures), the numerically calculated pressure jump in the liquid varies from that in the gas by 7% on the average. This represents acceptable agreement since the uncertainty in $\left[\frac{\Delta p}{p_0}\right]_{GAS}$ is about 10%. For these same four cases, the Khalatnikov results differ by an average of 19% from the pressure jumps in the vapor. The discrepancies for the three higher temperature cases are more serious with the numerical and Khalatnikov results differing on average from the gas jumps by 20% and 33%, respectively.

The poorer agreement between experiment and theory for the higher temperature cases may be the result of greater evaporation rates for these cases than for the lower temperature cases. As can be seen from table 3-3, the counterflow velocity, w, induced by the liquid pressure shock in the three higher temperature cases is positive, which here means toward the surface of the liquid. This also means that the initial heat flux produced is toward the surface in these cases. As a result, the temperature raising wave (which in these cases will be a fan and not a shock since the denominator of equation (2-2a) is negative above 1.88 °K) following the pressure shock into the liquid has its net ability to convect heat away from the hot surface degraded. The evaporation rates should therefore be higher for these cases which will tend to strengthen the reflected gasdynamic shock.

Table 3-3 compares the experimentally measured and the numerically calculated temperature jump across the transmitted liquid pressure shocks. The temperature measurements were obtained with superconducting sensors in conjunction with their static calibration curves. Also shown in the right- most column are the calculated counterflow velocities normalized by the upstream

first sound speed.

Experimental data for temperature shocks (Torczynski, 1982) may also be compared to the results from the shock program. Figure 3-4 shows the experimentally measured and calculated temperature jumps $\Delta T/T_0$ as a function of temperature shock Mach number M for an initial state set at T_0 = 1.609°K and $p_0 = SVP$. At each data point (circle), 95% of the value (cross) is also plotted, and it is apparent that up to $M \approx 1.04$ there is a constant 5% disagreement between experiment and calculation. This is most likely the result of the calibration procedure used for temperature sensor measurements of the second sound shock amplitude. However, the experimental data for $M > 1.04$ start to show significant disagreements with the numerical result. The data from this region, where the counterflow velocity w is large, may be of use in improving the therodynamics for helium II. Specifically, the second-order approximate equation (1-23) for the chemical potential follows from the exact differential relation (1-14) on the assumption that for small w, the normal fluid fraction ρ_n/ρ is approximately independent of w. Thus, what is meant by an improved thermodynamics is a better functional relation between the magnitude of w and ρ_n/ρ. It may also be true that the data from higher Mach nuber temperature shocks cannot be accounted for by the therodynamics alone, and that higher order w terms in the fundamental conservation equations are also necessary.

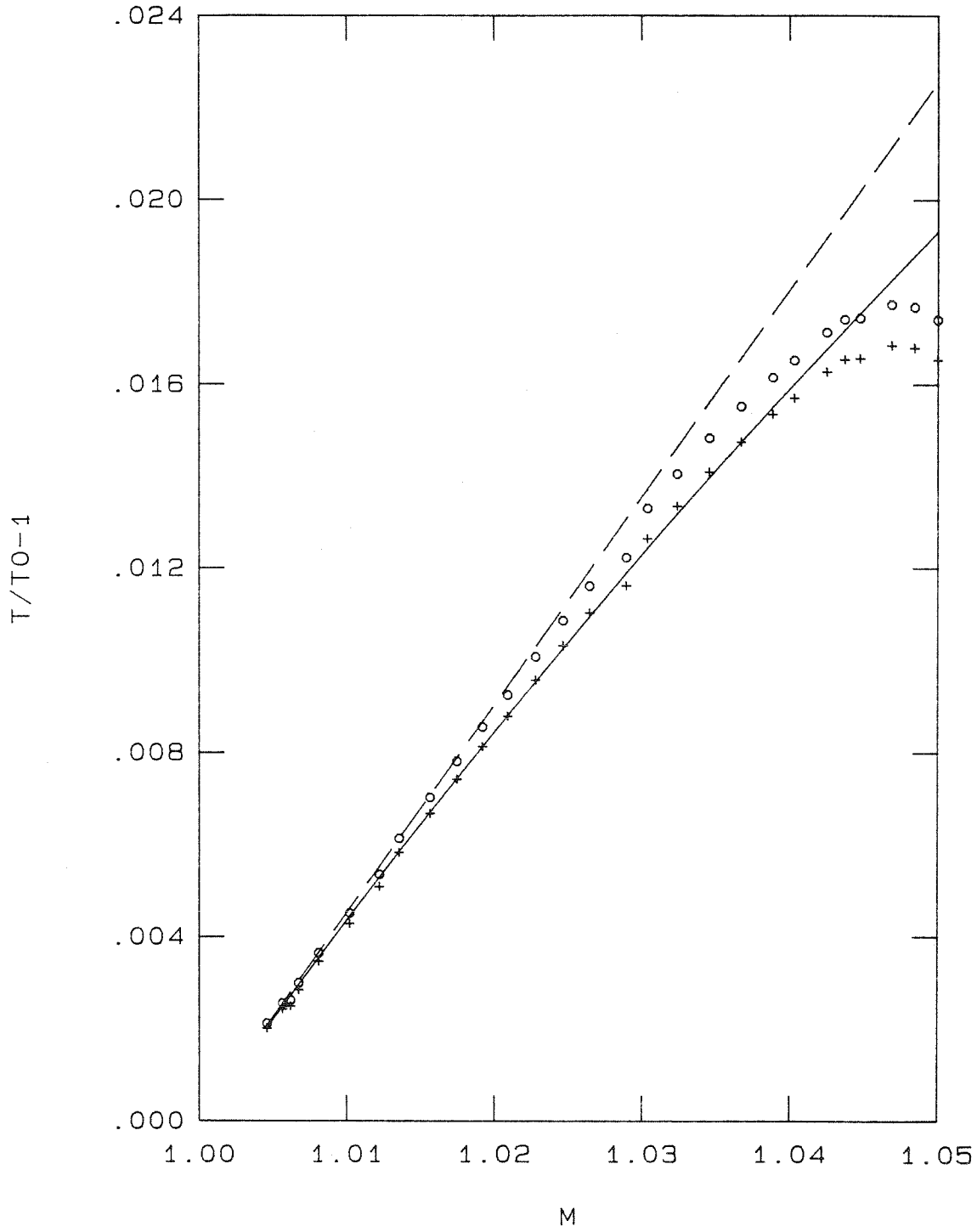

Figure 3-4. Temperature Jumps across Temperature Shocks for T_0 = 1.609 K and p_0 = *SVP*.

——— Numerical Result
— — — Khalatnikov Approximation
o Experimental Measurement
\+ 95% of Measured Value

Chapter 4

CONCLUSIONS

A computer program was developed to iteratively solve the shock jump conditions which follow from the Landau equations for superfluidity. The quality of thermodynamic state information used to supplement these equations allowed convergent shock solutions to be obtained for shock Mach numbers as low as 1.001 for temperature shocks and 1.004 for pressure shocks.

Comparisons of the numerical results to the Khalatnikov approximations can be summarized for the three basic cases: pressure shocks, temperature raising shocks, and temperature lowering shocks.

For pressure shocks, the numerically computed pressure jump exceeds Khalatnikov's approximation for stronger waves. Khalatnikov approximates pressure shocks as isothermal processes while the numerical solution shows a negative ΔT. The counterflow velocity w is zero by Khalatnikov, but actually is away from the shock for low Mach numbers and toward it for higher Mach numbers. The entropy and entropy flux jumps are virtually the same and both positive.

Temperature raising shocks show a positive sloping Hugoniot since the volume change is dominated by temperature change and not by compression. The magnitudes of the temperature increase and the pressure decrease across these shocks are smaller than the Khalatnikov values for strong waves. The counterflow velocity of the shocked liquid is always directed toward the shock and smaller in magnitude than the Khalatnikov value. The entropy and entropy flux jumps are both positive.

Temperature lowering shocks have temperature and pressure decreases across them which exceed in magnitude those given by Khalatnikov. The counterflow velocity of the shocked liquid is directed away from the shock, indicating a reversible heat extraction in the shocked region. As a consequence, the entropy decreases across such waves, but the entropy flux increases as it should according to the second law of thermodynamics.

Comparisons of the calculations to experimental data for pressure shocks reveal agreement superior to the Khalatnikov approximation in all cases. At lower temperatures the numerical results differ from the data by 7% on average. This represents acceptable agreement since the experimental precision is approximately 10%. At temperatures closer to the lambda line, where w is toward the liquid-vapor interface, the numerical results for Δp in the liquid are on average 20% lower than those calculated from shock speed measurements in the vapor. This is most likely the result of evaporative effects at the liquid surface.

Comparisons of these results to temperature shock data show good agreement for low Mach numbers. The data for higher Mach numbers show significant disagreement with the current two-fluid system of dynamic and thermodynamic equations. These data can possibly be used, in conjunction with a modified version of the superfluid shock wave program, to improve the two-fluid model.

PART II
EXPERIMENTAL INVESTIGATION OF THE LIQUID HELIUM II - VAPOR INTERFACE

Chapter 1

INTRODUCTION

The formulation of a complete and correct set of macroscopic boundary conditions for the liquid-vapor interface of helium II has been for some years and continues to be the object of many experimental and theoretical research efforts in low temperature physics. A particularly important problem for which knowledge of these boundary conditions is necessary is that of reflection from the liquid-vapor interface of a weak temperature shock wave. The $x-t$ diagram for such a problem is shown in Figure 1-1. All of the waves are assumed sufficiently weak so as to be considered linear; their speeds are therefore all approximately sonic. Thus a_1, a_2, and a_g represent the liquid first sound speed, second sound speed, and the gas sound speed, respectively. The incident temperature shock, processing the liquid from state 1 to state 2, produces three subsequent waves as it impinges upon the liquid surface. Firstly, a pressure wave is transmitted into the vapor due to evaporation from the surface, and it processes the gas from state 0 to state 6. As the liquid evaporates, the interface position (shown by the dashed line) recedes into the liquid with speed $\dot{X}$. The gas processed by the transmitted wave in the vapor (state 6), and that which has evaporated from the liquid surface (state 5) are separated by a contact surface indicated by the dotted line. Pressure and velocity are continous across this surface but temperature, as will be shown, is not. Secondly, the pressure rise produced by the transmitted wave causes a pressure wave of equal strength to reflect into the liquid, processing it from state 2 to state 3. Finally, the third wave produced is a reflected temperature shock which processes the liquid from state 3 to state 4. Importantly, the incident temperature wave does not change sign upon reflection from the vapor boundary; i.e., the vapor appears thermally

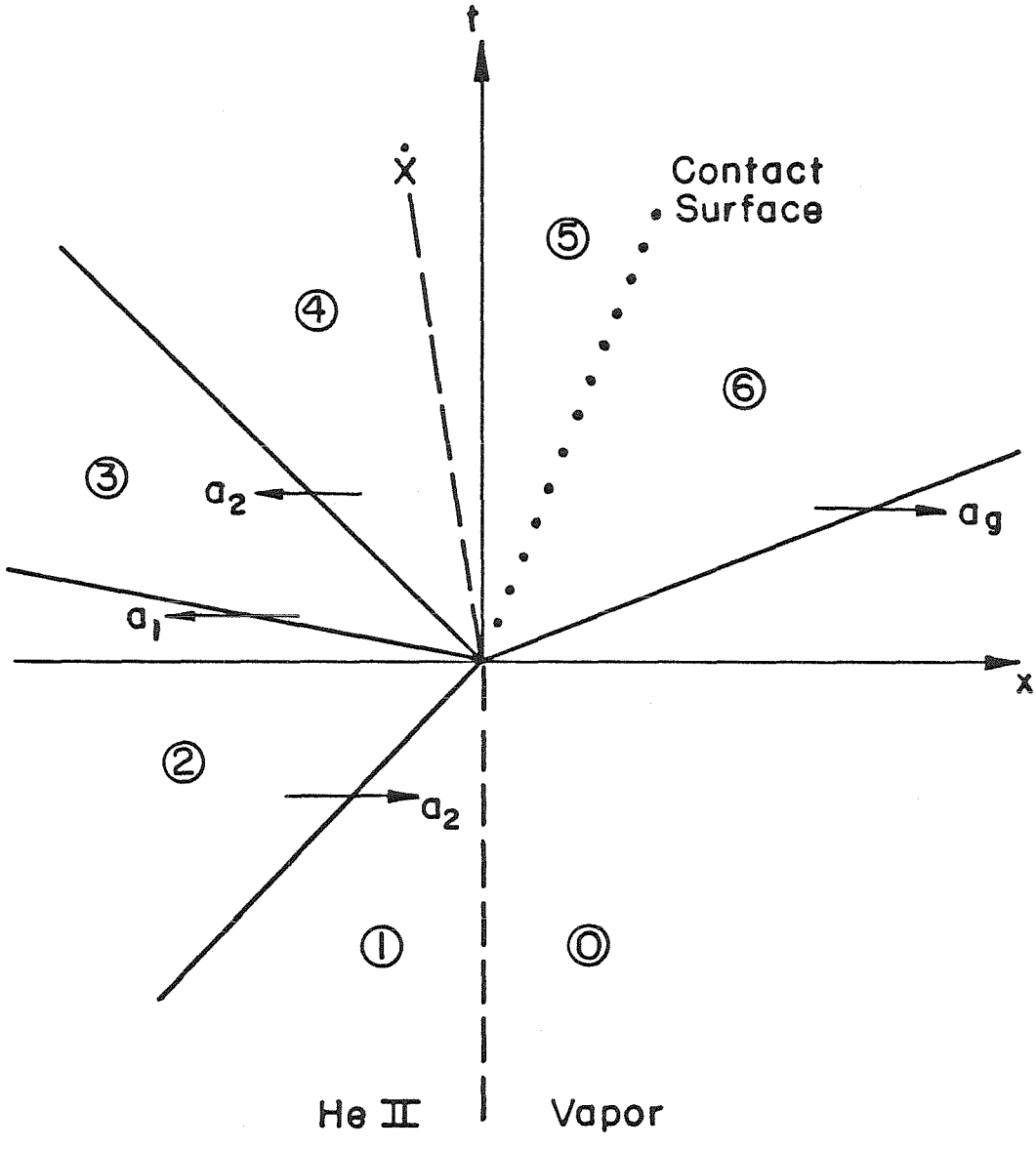

Figure 1-1. x-t Diagram for Weak Temperature Shock Reflection from He II - Vapor Interface

"hard" in analogy to an acoustically hard surface for pressure waves. Physically, this can be traced to the analogy between heat flux for second sound (temperature waves) and mass flux for first sound (pressure waves). A mechanically rigid, i.e., acoustically hard, surface sets a boundary condition of near zero mass flux, and pressure waves reflect from such a surface without sign change. To second sound, all boundaries appear thermally "hard" because their only mode of heat transport is conduction, and this is far inferior to helium II's convective heat flux mode associated with its counterflow velocity.

For an incident linear temperature wave of known strength, the strengths of the transmitted and reflected waves are desired. That is, given the initial undisturbed states in regions 0 and 1, and the state 2 produced by the incident wave, we wish to calculate all of the subsequent states in regions 3 through 6. To begin, conservation of mass, momentum, and energy require the fluxes of these quantities to match in steady state. For times which are long compared to the reflection time, the flow relative to the interface in regions 4 and 5 can be considered steady. Therefore, matching fluxes across the interface gives:

mass:

$$(\rho u)_4 = (\rho u)_5 = j$$

momentum:

$$\left[\rho u^2 + \frac{\rho_s \rho_n}{\rho} w^2 + p\right]_4 = (\rho u^2 + p)_5$$

energy:

$$\left[j\left[h + \frac{1}{2}u^2 \right] + \rho_s\, sTw + \left[1 - \frac{1}{2}\frac{\rho_n}{\rho} \right] w^2\, \rho_n\, u + \frac{\rho_s}{\rho}\left[wu + \frac{\rho_s}{\rho} w^2 \right] \rho_n\, w \right]_4$$

$$= \left[j\left[h + \frac{1}{2}u^2 \right] \right]_5$$

Linearization of these equations gives:

$$(\rho u)_4 = (\rho u)_5 = j$$

$$p_4 = p_5$$

$$jh_4 + (\rho_s sTw)_4 = jh_5$$

or, upon transforming from interface coordinates to a fixed system

$$\rho_4 (u_4 - \dot{X}) = \rho_5 (u_5 - \dot{X}) = j \qquad (1\text{-}1)$$

$$p_4 = p_5 \qquad (1\text{-}2)$$

$$jL = (\rho_s sTw)_4 \qquad (1\text{-}3)$$

where L has been used for the latent heat of vaporization.

$$L = h_5 - h_4$$

The weak coupling between first and second sound will be neglected, and the following equalities will hold.

$$p_0 = p_1 = p_2$$

$$T_0 = T_1$$

$$T_2 = T_3$$

$$p_3 = p_4 = p_5 = p_6$$

$$u_5 = u_6$$

The densities, temperatures, and pressures in regions 4 and 5 have been only slightly perturbed from their equilibrium values, and these perturbations are linearly related to the velocities as follows:

$$u_5 = \frac{(p_5 - p_0)}{\rho_0 a_g} \tag{1-4}$$

$$u_4 = -\frac{(p_4 - p_1)}{\rho_1 a_1} \tag{1-5}$$

$$w_4 = \left[\frac{\rho s}{\rho_n a_2}\right]_1 \left[(T_2 - T_1) - (T_4 - T_2)\right] \tag{1-6}$$

In equation (1-6) the thermal hardness of the vapor has been used to assign the proper direction to the reflected counterflow velocity. Using equations (1-4) through (1-6) to replace the velocities in equations (1-1) through (1-3), and letting

$$p_4 - p_1 = p'$$

$$p_5 - p_0 = p_g'$$

$$T_2 - T_1 = T_i'$$

$$T_4 - T_2 = T_r'$$

gives

$$\rho_1 \left[-\frac{p'}{\rho_1 a_1} - \dot{X}\right] = \rho_0 \left[\frac{p_g'}{\rho_0 a_g} - \dot{X}\right] = j \tag{1-7}$$

$$p' = p_g' \tag{1-8}$$

$$j\,L = \left[\frac{\rho_s\, \rho\, s^2\, T}{\rho_n a_2}\right]_1 \left[T_i' - T_r'\right] \tag{1-9}$$

Now the gas pressure perturbation p_g' is related to the temperature perturbation $T_g' = T_g - T_0$ by the isentropic ideal gas relation

$$\frac{p_g'}{T_g'} = \frac{\gamma}{\gamma - 1} \frac{p_0}{T_0} \tag{1-10}$$

where γ is the specific heat ratio in the vapor.

Substituting equation (1-8) into (1-7) and eliminating $\dot{X}$ gives

$$j = (1 + \varepsilon) \frac{p_g'}{a_g} \tag{1-11}$$

where

$$\varepsilon = \frac{a_g/a_1 + 1}{\rho_1/\rho_0 - 1}$$

and is a small number since $\rho_1 >> \rho_0$. Now, substituting equations (1-10) and (1-11) into (1-9) and using $p_0 = p_1$, $T_0 = T_1$ gives

$$T_g' = Q(T_i' - T_r') \tag{1-12}$$

where

$$Q = \left[\frac{1}{1 + \varepsilon}\right]\left[\frac{\gamma - 1}{\gamma}\right] \frac{\rho_1 s_1^2 T_1^2}{p_1 L} \frac{\rho_s}{\rho_n} \frac{a_g}{a_2} . \tag{1-13}$$

Equation (1-12) relates the strengths of the transmitted pressure wave and reflected temperature wave, but further equations are required to give separate

expressions for each.

If the evaporation proceeds very slowly, i.e., the mass flux is very small, then thermodynamic equilibrium should exist between regions 4 and 5. This implies equality of chemical potentials and temperatures.

$$\mu_4 = \mu_5 \tag{1-14}$$

$$T_4 = T_5 \tag{1-15}$$

But even with reversible evaporation, the temperature in region 5 exceeds that in region 6, which may be proved as follows.

$$s_6 = s_0$$

$$= L / T_0 + s_1$$

$$= s_5 - s_4 + s_1$$

$$< s_5$$

Thus

$$T_6 < T_5 \ .$$

It is in the third step of the proof that reversibility has been used to express the latent heat simply in terms of the entropy difference between the phases since

$p_4 = p_5$ and $T_4 = T_5$. The temperature inequality follows immediately from the entropy inequality since entropy is always a monotonically increasing function of temperature. Letting

$$T_5 = T_6 + \theta_g = T_1 + T_g' + \theta_g$$

equations (1-14) and (1-15) may be written as

$$-s_1 (T_i' + T_r') + \frac{p'}{\rho_1} = -s_0 (T_g' + \theta_g) + \frac{p_g'}{\rho_0} \tag{1-16}$$

$$T_i' + T_r' = T_g' + \theta_g \tag{1-17}$$

where use has been made in (1-16) of the identity $d\mu = -sdT + (1/\rho)dp$. Using equations (1-8) and (1-10), equations (1-16) and (1-17) may be combined to give

$$T_g' = \frac{\rho_1 \rho_0}{\rho_1 - \rho_0} \frac{\gamma - 1}{\gamma} \frac{L}{p_1} (T_i' + T_r') \tag{1-18}$$

Combining equations (1-12) and (1-18) gives

$$R = \frac{D-1}{D+1} \tag{1-19}$$

where

$$R = T_r'/T_i' \tag{1-20}$$

and

$$D = \left[\frac{1}{1+\varepsilon}\right]\left[\frac{\rho_1 - \rho_0}{\rho_0}\right]\left[\frac{s_1 T_1}{L}\right]^2 \frac{\rho_s}{\rho_n}\frac{a_g}{a_2} . \qquad (1\text{-}21)$$

An expression for the reflection coefficient has now been obtained, based on the assumption that the interface is in approximate equilibrium. However, it is of interest to note that, in contrast to the interface wave reflection problem for a classical fluid, linearity in the helium II problem does not automatically imply equilibrium. True equilibrium between phases exists if and only if the mass flux j relative to the interface is negligible, i.e. zero within the linear approximation. The linearized energy equation (1-3) shows this to be the case for the classical fluid ($w = 0$), but for helium II, the heat flux associated with counterflow is of the same order as the mass flux. Thus the wave strength of the incident weak second sound shock is of the same order as the evaporation rate which it produces. Therefore, by reducing the strength of the incident temperature shock, one is by no means assured of more closely approaching an equilibrium interface.

1.1. Previous Investigations

The experiments of Wise (1979) provided the original motivation for investigating the effects of evaporation from the He II interface. In these experiments, a gasdynamic shock wave moving with velocity U_s reflects from the liquid surface, producing a reflected shock, transmitted pressure and temperature shocks, and an interface velocity, $\dot{X}$. (See Figure 1-2.) All wave velocities U_s, U_R, c_1, and c_2 were measured as well as $\dot{X}$. Upon computing the particle velocity u_5 behind the reflected shock from ideal gas jump conditions and u_6 in the liquid from the program described in Part I, it is always found that

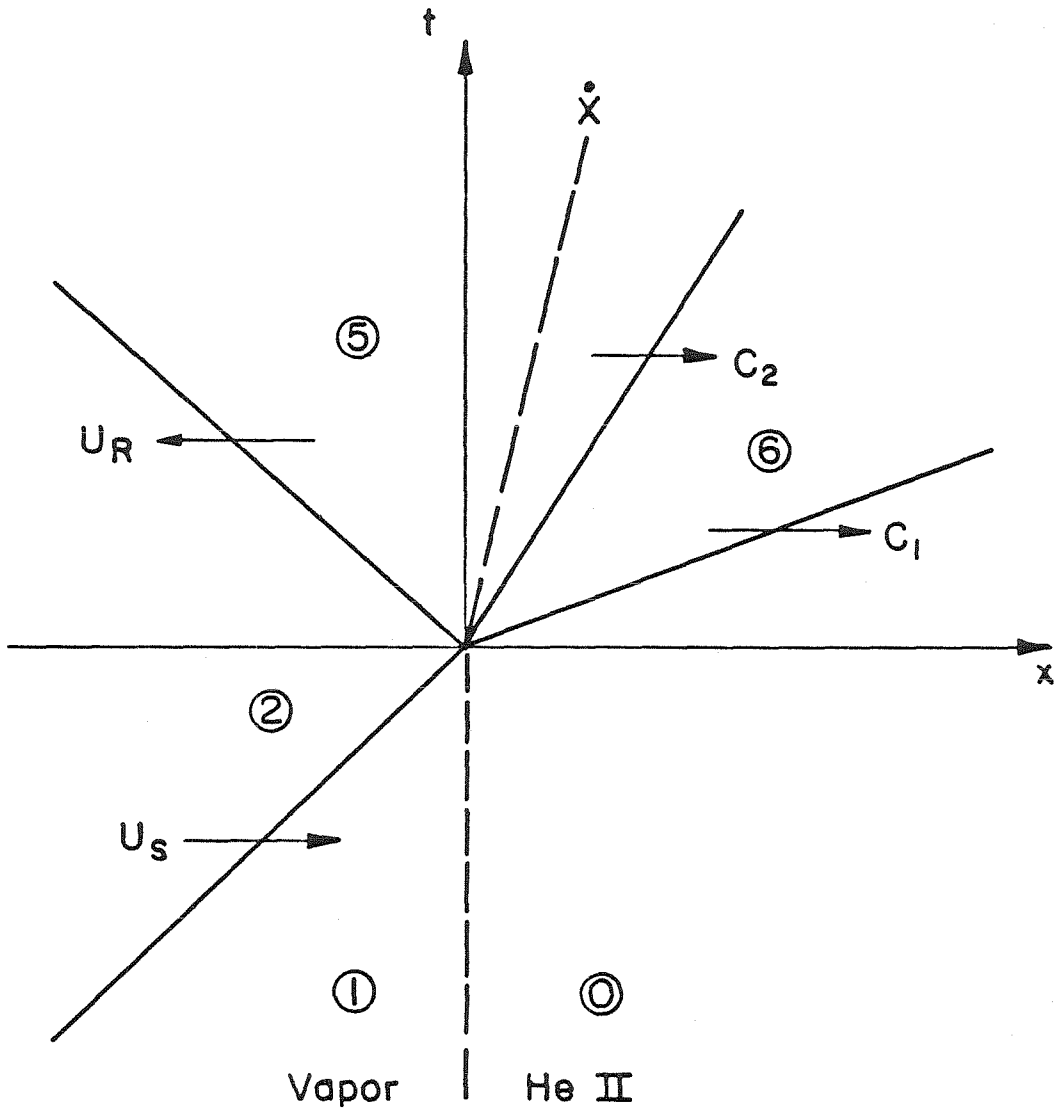

Figure 1-2. x-t Diagram for Gasdynamic Shock Reflection from He II - Vapor Interface

$$u_5 < \dot{X} < u_6 \ .$$

In fact, in some cases, u_5 is negative (away from the liquid surface) whereas $\dot{X}$ is always positive. (See Table 1-1.)

Table 1-1. Velocities Produced by Gasdynamic Shock Reflection from He II - Vapor Interface

Exp't	T_0(K)	p_0	u_5(m/sec)	$\dot{X}$(m/sec)	u_6(m/sec)
a	1.522	SVP	-59.0	10.6	18.2
b	1.665	"	3.30	8.6	14.7
c	1.751	"	-71.4	12.3	20.6
d	1.832	"	-14.5	9.96	23.2
e	1.989	"	1.05	10.2	19.5
f	2.031	"	-29.9	11.1	18.5
g	2.095	"	-18.7	11.2	29.0

This velocity discontinuity suggests an evaporating interface. Since the waves measured by Wise are all strongly nonlinear, it was deemed desirable to experimentally study evaporation induced by weak temperature shocks incident from the liquid side of the interface rather than by strong shocks so as to isolate evaporative effects from nonlinear ones.

Hunter and Osborne (1969) measured the reflection coefficient R for second sound for 1.0°K < T_0 < 1.8°K. Heat pulses were generated in the liquid by supplying current pulses to a thin metal film at the base of a tube 1 cm in diameter

and of variable length (7 cm to 14 cm). The receiving sensor was a thin carbon layer 2 mm wide and 4 mm long painted on the interior wall of the tube equidistant from the heater at the base and the open top end. The heater pulses were of 400 μs duration, were repeated at rates from 1 Hz to 4 Hz, and produced heat fluxes of up to 1 W/cm^2. For the temperatures investigated, they measured $R \approx 0.80$.

Buchholz, Brandt, and Wiechert (1971) measured R for 1.26°K < T_0 < 2.17°K. The second sound wave was produced by exciting a carbon layer with 4 periods of a 10 kHz alternating current. The heat flux produced was 150 mW/cm^2. The tube was 6 cm long and had a square cross sectional area of 1 cm^2. The receiver was a superconducting aluminum film 0.1 mm wide and 10 mm long. As with the measurements of Hunter and Osborne, they found $R \approx 0.80$ for T < 2.0°K, but above 2.0°K, R was found to rapidly decrease.

1.2. Objective of the Present Work

Because the reflection coefficient computed according to equations (1-19) and (1-21) is roughly 20% below that measured by the above authors, much effort has been devoted to developing models which explain this discrepancy. (See, for example, Wiechert (1980).) The purpose of this effort was first to more precisely measure R with newer techniques. However, the more important purpose was to also measure the transmission coefficient $\overline{T} = T_g'/T_i'$. This would provide a check on the fundamental equation (1-12) which does not contain any assumptions about an equilibrium interface, but only requires linearity in the conservation equations. Measurement of both R and $\overline{T}$ is equivalent to measuring Q directly, and from equation (1-13)

$$Q \approx \frac{\gamma-1}{\gamma} \frac{\rho_1 s_1^2 T_1^2}{p_1 L} \frac{\rho_s}{\rho_n} \frac{a_g}{a_2} . \qquad (1\text{-}22)$$

This same dimensionless grouping appears when one solves the complementary problem of a sound wave incident from the vapor reflecting from the liquid surface. With Q being given by (1-22), the wave amplitudes in this case are related by the following equation.

$$Q\ T_l' = \left[T_i' - T_r'\right] \tag{1-23}$$

Here, T_l' is the temperature perturbation produced by the transmitted second sound wave. The directly measured values for Q were then to be compared against the expression given in (1-22) as well as values computed from Wise's data via (1-23).

Chapter 2

EXPERIMENTS

2.1. Apparatus Description

Figure 2-1 shows a cross sectional schematic of the apparatus which was constructed to measure the reflection and transmission coefficients. A brass tube, 5.2 inches high with a 1.25 inch inside diameter had clamped to its base a quartz disc of 2.0 inch diameter. Centered on the top face of this disc was an evaporated nichrome film, 1000 Å thick and 1.375 inches wide. Copper leads of 2000 Å thickness were evaporated over the ends of the nichrome strip leaving exposed a nichrome square having a 1.375 inch side. A bevelled ring of teflon formed a seal between the nichrome film and the end of the brass tube. D.C. current pulses through this film produced heat flux densities of 1.9 W/cm^2. The pulses were of 250 μs duration.

A brass piece was machined to fit within the tube and provide a mount for three temperature sensors. The lowest sensor, shown immersed in the liquid, was sidewall mounted and used to measure the incident and reflected second sound shock strengths, T_i' and T_r', respectively. The two upper sensors were endwall mounted and used to measure the temperature perturbation produced by the transmitted pressure wave and its time of flight between these two stations. The three sensors were approximately equally spaced vertically, being separated by 1.5 inch intervals. They each consisted of a thin, superconducting film evaporated onto a glass coverslip. The film itself was fabricated by evaporating 200 Å of gold onto the glass followed by 800 Å of tin onto the gold. Films made in this way transition from normal to superconducting at approximately 2.0 °K in the absence of a magnetic field. A small electromagnet with a

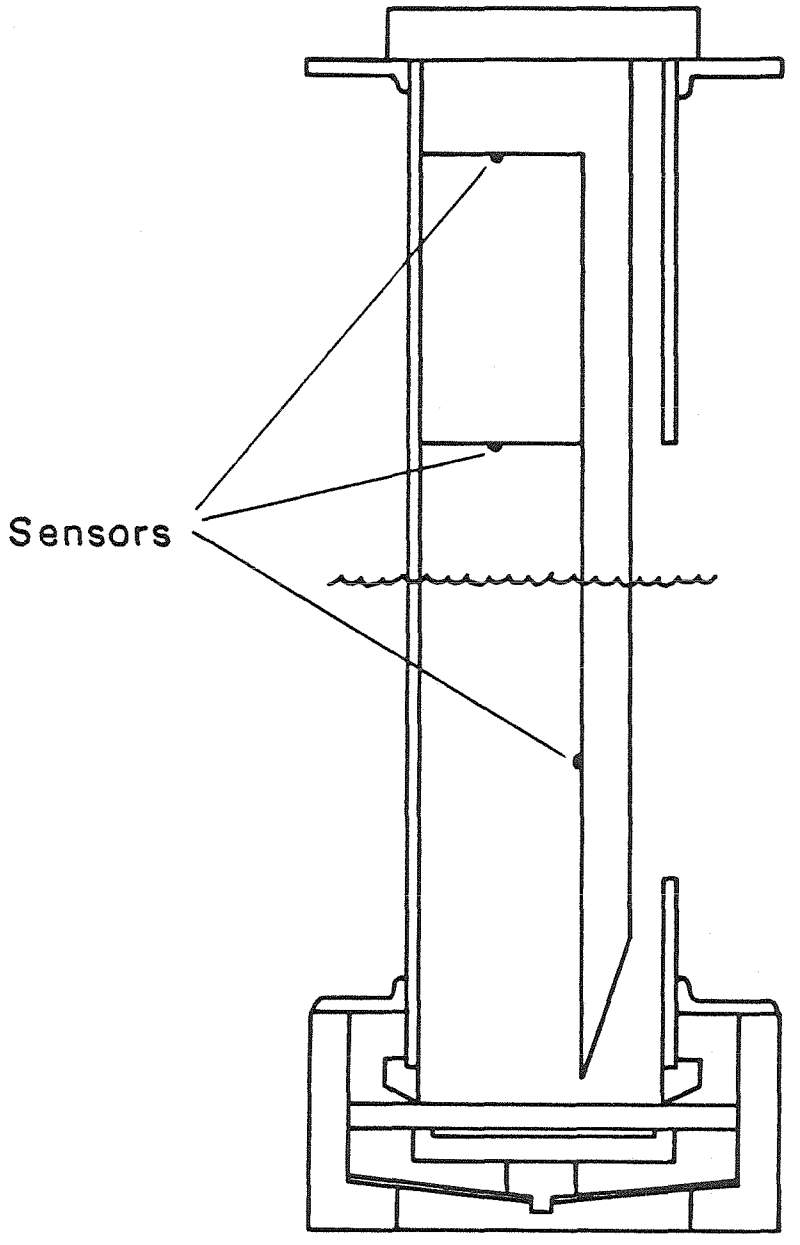

Figure 2-1. Experimental Apparatus

core machined from Armco (50% nickel and 50% iron alloy) and wrapped with several thousand turns of superconducting Niobium-Titanium wire was positioned behind the glass substrate of each sensor in order to adjust the sensor transition temperature to the operating temperature of the experiment. The room temperature resistance of these sensors was approximately 300 ohms, falling to approximately 50 ohms at 4 °K. Supplied with a 1 mA D.C. current, they typically showed sensitivities of 0.3 V/°K. The apparatus was suspended within the dewar and positioned relative to the interface by braided stainless steel fishing line. Prior to being placed into the dewar, the entire apparatus was surrounded by aluminum foil to shield it from room lights.

2.2. Experimental Procedure

Experiments were performed at three temperatures T_0 on the saturated vapor pressure curve: 1.500, 1.765, and 1.989 °K. With all three sensors immersed in the liquid, the distance between the upper two was accurately determined with a method suggested and used previously by Turner (1979). The speed with which a weak temperature shock propagates is linearly related to its strength. In turn, the strength is proportional to V^2, the square of the voltage applied to the heater. Thus, if the inverse of the time of flight, $(\Delta t)^{-1}$, between the two sensors is plotted versus V^2 , a straight line results. Extrapolating to zero voltage gives the time taken to traverse the distance by a disturbance travelling at the speed of second sound, a_2 . Since a_2 is rather accurately known (see Maynard (1976)), the length is determined to comparable accuracy. A distance of 3.795 cm was established in this way and corresponds quite closely to the measured room temperature length corrected for the thermal contraction of brass.

Prior to taking data, the magnets were adjusted to give a voltage drop of approximately 12 mv across each sensor. This was approximately one fourth of

the voltage drop for the fully normal state at 4 °K, and provided an operating point at the lower end of the most linear portion of the transition curve. For each sensor, voltage drop as a function of saturated vapor pressure was then plotted with an X-Y recorder to give calibration curves necessary to convert voltage changes to temperature changes. All sensors were calibrated in the liquid because calibrations done in the vapor showed a hysteresis, i.e., curves traced out as the temperature rose showed different transition temperatures from those obtained by pumping down slowly.

When taking data, the middle sensor was less than 3 mm above the liquid surface and shocks were fired at approximately one minute intervals. The voltage pulses resulting at the sensors upon arrival of the waves were amplified and used as input to an oscilloscope and to counters, which recorded time elapsed since the heater pulse. Photographs of the oscilloscope trace provided wave amplitude records.

2.3. Results

Measurements of the length between the two upper sensors and arrival times gave the wave speed of the pressure pulse in the vapor. The pressure perturbation p_g' produced by this wave is related to the Mach number M by the ideal gas jump condition

$$\frac{p_g'}{p_0} = \frac{2\gamma}{\gamma+1}(M^2 - 1). \qquad (2\text{-}1)$$

Unfortunately, this pressure wave produced by evaporation was sufficiently weak so as to travel sonically within the precision limitations of not only these experiments but also of previous measurements of the sound speed in low temperature helium vapor. (See, for example, McCarty (1980).) Time of flight

measurements were therefore of no use in deducing the strength, p_g'.

Table 2-1 shows the experimental results for the coefficients $R_{EXP} = (T_r'/T_i')_{EXP}$ and $\bar{T}_{EXP} = (T_g'/T_i')_{EXP}$ based on amplitude measurements.

Table 2-1. Experimental Results

T_0(K)	R_{EXP}	$\bar{T}_{EXP}$	Q_{EXP}	Q_{TH}
1.500	0.84	0.62 (middle sensor)	3.88	13.53
1.500	0.84	0.93 (upper sensor)	5.81	13.53
1.765	0.84	0.73 (middle sensor)	4.56	11.63
1.989	0.76	0.68 (middle sensor)	2.83	9.89

These measurements imply by equation (1-12) values for Q given by

$$Q_{EXP} = \bar{T}_{EXP} / (1 - R_{EXP}) \tag{2-2}$$

which may be compared to Q predicted by equation (1-13) as

$$Q_{TH} = \left[\frac{1}{1+\varepsilon}\right]\left[\frac{\gamma-1}{\gamma}\right]\frac{\rho_1 s_1^2 T_1^2}{p_1 L}\frac{\rho_s}{\rho_n}\frac{a_g}{a_2} . \tag{2-3}$$

The measured values of R should be reliable since they are obtained simply as the ratio of the height of two oscilloscope traces for the same sensor (the

lowest of the three), and sensor response and calibration in the liquid are highly repeatable.

However, many questions arise about the reliability of measurements in the vapor. As shown, the values of $\overline{T}$ measured at the upper and middle sensors in the first experiment (T_0 = 1.5 °K) differ by 50%. At T_0 = 1.989 °K, the upper sensor would transition to its full normal state when its magnet was turned on, and therefore could not be used at all. Table 2-1 also shows Q_{TH} to exceed Q_{EXP} by as much as a factor of 3.5. One possible reason for this is the film of helium II which coats the sensors in the vapor, and itself produces a liquid-vapor interface through which the vapor pulse must pass. Reflection from the film surface thus results in incomplete transmission to the sensor, which gives a spuriously low value for $\overline{T}$. Note that measurement of Q requires measurement of three wave amplitudes: incident, reflected, and transmitted. Since Q is assumed the same for the film as for the bulk liquid, it might be supposed that equations (1-23) and (1-12) could be combined in a way which would allow determination of Q from the three amplitudes which can be measured. But this is not the case because the three amplitudes must refer to the same interface. The incident and reflected waves measured by the submerged sensor come from interactions at the bulk liquid-gas interface. The amplitude of the wave transmitted into the gas toward the film coated sensor in the vapor cannot be directly measured. This wave becomes the incident wave for the gas-film interface, but its amplitude is unknown. In fact, all that can be measured as a result of interactions at this interface is the second sound wave amplitude which is transmitted to the sensor. Thus, in the original problem, to which (1-12) applies, the equation contains two unknowns, Q and the transmitted wave strength. For the film problem, to which (1-23) applies, the equation contains three unknowns, Q and the incident and reflected wave strengths. These observations, together with the previously mentioned problem of sensor calibration in the vapor, force one to

conclude that these experiments failed to produce reliable values for the transmission coefficient for second sound by either wave speed or amplitude measurements. To the author's knowledge, results for this coefficient have not been published as of this writing.

The measurements of R may be compared to previous work. The paper of Hunter and Osborne (1969) gives $R = 0.78$ at $T_0 = 1.47$ °K and $R = 0.80$ at $T_0 = 1.75$ °K. Buchholz, Brandt, and Wiechert (1971) report $R = 0.78$ at $T_0 = 1.47$ °K, $R = 0.77$ at $T_0 = 1.75$ °K, and $R = 0.80$ at $T_0 = 1.99$ °K. The former authors make no statement regarding the precision of R measurements, while the latter estimate ± 0.05 in these temperature ranges. The estimate for this work is also ± 0.05 and these data thus reproduce the measurements of the previous authors.

The reflection coefficient as calculated from equilibrium theory by equations (1-19) and (1-21) gives values of R which are roughly 20% lower than measured. This discrepancy has yet to be explained by any physically reasonable model. The evaporating, nonequilibrium superfluid interface is still not well understood.

Chapter 3

CONCLUSIONS

An apparatus was constructed to measure the linear reflection and transmission coefficients for second sound incident upon the free liquid surface. Measurement of the transmitted wave amplitude failed due to precision limitations on velocity measurements and the superfluid film which coats the sensors in the vapor. Measurements of the reflection coefficient reproduced the work of previous authors. The high evaporation rate induced by second sound reflection produces a nonequilibrium interface, even for small amplitude waves. This nonequilibrium behavior is not presently well understood on a physically sound basis.

References

BAKER, S. 1982 Private communication.

BUCHHOLZ, F.I., BRANDT, D., & WIECHERT, H. 1971 *Phys. Letters* **35A**, 471.

CUMMINGS, J.C. 1973 Ph.D. Thesis, Calif. Inst. of Tech.

CUMMINGS, J.C. 1976 *J. Fluid Mech.* **75**, 373.

CUMMINGS, J.C., SCHMIDT, D.W., & WAGNER, W.J. 1978 *Phys. Fluids* **21**, 713.

DESSLER, A.J. & FAIRBANK, W.M. 1956 *Phys. Rev.* **104**, 6.

GOODSTEIN, D.L. 1975 **States of Matter**, Prentice-Hall, Englewood Cliffs, New Jersey.

GULYAEV, A.I. 1967 *JETP Letters* **5**, 325.

GULYAEV, A.I. 1970 *Sov. Phys. JETP* **30**, 34.

HUNTER, G.H. & OSBORNE, D.V. 1969 *J. Phys. C* **2**, 2414.

ISAACSON, E. & KELLER, H.B. 1966 **Analysis of Numerical Methods**, John Wiley & Sons, New York.

KHALATNIKOV, I.M. 1952 *Zh. Eksp. Theor. Fiz.* **23**, 253.

KHALATNIKOV, I.M. 1965 **Introduction to the Theory of Superfluidity**, Benjamin, New York.

LANDAU, L. 1941 *J. Phys. U.S.S.R.* **5**, 71.

LANDAU, L.D. & LIFSHITZ, E.M. 1959 **Fluid Mechanics**, Pergamon, London.

MAYNARD, J. 1976 *Phys. Rev. B* **14**, 3368.

McCARTY, R.D. 1980 *N.B.S. Tech. Note* **1029**.

OSBORNE, D.V. 1951 *Proc. Phys. Soc. Lond.* **64**, 114.

STURTEVANT, B. 1976 *Bul. Amer. Phys. Soc.* **21**, 1223.

TORCZYNSKI, J. 1982 Private communication.

TURNER, T.N. 1979 Ph.D. Thesis, Calif. Inst. of Tech.

WIECHERT, H. 1980 *J. Low Temp. Phys.* **39**, 623.

WISE, J.L. 1979 Ph.D. Thesis, Calif. Inst. of Tech.

Appendix A

CHEMICAL POTENTIAL CONSTRUCTION

As mentioned at the close of Chapter 2, the chemical potential was treated somewhat differently than the other thermodynamic variables since it requires the most computer time to construct. This is because the Gibbs-Duhem relation must be integrated from an established reference point, μ_0.

$$\mu - \mu_0 = -\int s dT + \int \frac{1}{\rho} dp \qquad \text{(A.1)}$$

For reasons of speed, it is not practical during the iterative shock calculations to integrate this relation from the same reference point each time. Thus, a lookup table consisting of 442 values for $\mu(p,T)$ was calculated for use as constants of integration, as follows. Starting from $\mu = -1.489157\times10^4\ m^2/sec^2$ at $T = 1.2°K$ and $p = 0$ bar, nineteen additional points along the zero isobar were calculated at intervals of 0.05°K. The integration of (A.1) to each successively higher temperature was accomplished by subdividing each interval into 20 equal parts and using Simpson's rule. Then, starting from the established zero pressure values, points were calculated along the isotherms (equally separated by 0.05°K) in increments of 1 bar up to the lambda line or melting line. Again, the integration of (A.1) to each successively higher pressure was done by Simpson's rule with the 1 bar increments divided into 20 equal subdivisions. The calculation was repeated in the same way along the isobars starting from $T = 1.2$°K up to the lambda line in increments of 0.05°K. The results from the constant pressure and constant temperature integrations (which differ at most by 1.2%) were then averaged to give the points which comprise the lookup table used by the

shock program. By using a value of μ_0 from this table closest to the pressure and temperature of interest, the shock program calculates $\mu(p,T)$ from (A.1) to sufficient accuracy in only one application of Simpson's rule. The table given by Maynard (1976) for $\mu(p,T)$ contains roughly half as many points as this new one given in Table A.1, and values of μ at identical pressures and temperatures in these two tables can differ by as much as 4.8%. The new table gives more reliable results during jump condition calculations for weak shock waves.

T(K)	p(bar)				
	0	1	2	3	4
1.20	14891.57	14207.10	13530.32	12860.64	12197.54
1.25	14894.51	14210.05	13533.29	12863.64	12200.59
1.30	14898.26	14213.82	13537.11	12867.51	12204.51
1.35	14903.00	14218.61	13541.95	12872.42	12209.51
1.40	14908.93	14224.59	13548.01	12878.58	12215.77
1.45	14916.27	14232.00	13555.52	12886.20	12223.52
1.50	14925.25	14241.07	13564.71	12895.53	12233.00
1.55	14936.13	14252.07	13575.84	12906.83	12244.49
1.60	14949.21	14265.27	13589.22	12920.40	12258.28
1.65	14964.79	14281.01	13605.15	12936.56	12274.69
1.70	14983.20	14299.60	13623.97	12955.64	12294.07
1.75	15004.81	14321.42	13646.05	12978.02	12316.78
1.80	15030.02	14346.87	13671.80	13004.12	12343.26
1.85	15059.25	14376.38	13701.65	13034.36	12373.93
1.90	15092.97	14410.42	13736.08	13069.23	12409.30
1.95	15131.71	14449.51	13775.62	13109.28	12449.92
2.00	15176.03	14494.25	13820.88	13155.14	12496.45
2.05	15226.60	14545.33	13872.58	13207.57	12549.69
2.10	15284.26	14603.64	13931.69	13267.60	12610.75
2.15	15350.30	14670.55	13999.72		

Table A.I. Chemical potential. Entries are $-\mu(p,T)(m^2/sec^2)$

T(K)	p(bar)				
	5	6	7	8	9
1.20	11540.58	10889.39	10243.63	9603.03	8967.33
1.25	11543.67	10892.53	10246.83	9606.29	8970.65
1.30	11547.67	10896.60	10250.98	9610.53	8974.99
1.35	11552.75	10901.79	10256.28	9615.94	8980.53
1.40	11559.13	10908.29	10262.92	9622.73	8987.48
1.45	11567.03	10916.34	10271.14	9631.13	8996.07
1.50	11576.68	10926.19	10281.19	9641.39	9006.56
1.55	11588.38	10938.10	10293.34	9653.80	9019.23
1.60	11602.41	10952.39	10307.90	9668.65	9034.40
1.65	11619.09	10969.37	10325.20	9686.29	9052.40
1.70	11638.78	10989.41	10345.60	9707.08	9073.60
1.75	11661.87	11012.88	10369.49	9731.42	9098.41
1.80	11688.75	11040.21	10397.30	9759.74	9127.27
1.85	11719.89	11071.86	10429.49	9792.52	9160.67
1.90	11755.80	11108.35	10466.61	9830.30	9199.18
1.95	11797.04	11150.26	10509.25	9873.73	9243.45
2.00	11844.30	11198.32	10558.17	9923.58	9294.31
2.05	11898.43	11253.42	10614.34	9980.91	9352.93
2.10	11960.64	11316.93			

Table A.I. (Continued)

T(K)	p (bar)				
	10	11	12	13	14
1.20	8336.30	7709.74	7087.44	6469.21	5854.89
1.25	8339.70	7713.21	7091.00	6472.86	5858.63
1.30	8344.14	7717.76	7095.66	6477.64	5863.54
1.35	8349.81	7723.57	7101.62	6483.76	5869.82
1.40	8356.93	7730.86	7109.09	6491.43	5877.69
1.45	8365.72	7739.87	7118.32	6500.89	5887.41
1.50	8376.45	7750.85	7129.57	6512.43	5899.24
1.55	8389.41	7764.11	7143.14	6526.33	5913.49
1.60	8404.90	7779.95	7159.35	6542.92	5930.49
1.65	8423.28	7798.73	7178.56	6562.58	5950.63
1.70	8444.92	7820.84	7201.15	6585.70	5974.29
1.75	8470.23	7846.68	7227.57	6612.71	6001.94
1.80	8499.67	7876.73	7258.27	6644.11	6034.08
1.85	8533.73	7911.51	7293.80	6680.44	6071.28
1.90	8573.01	7951.61	7334.79	6722.38	6114.24
1.95	8618.19	7997.76	7381.99	6770.72	6163.81
2.00	8670.14	8050.91	7436.45	6826.61	6221.31
2.05	8730.19	8112.58			

Table A.I. (Continued)

T(K)	p(bar)				
	15	16	17	18	19
1.20	5244.31	4637.31	4033.75	3433.51	2836.47
1.25	5248.14	4641.25	4037.80	3437.67	2840.74
1.30	5253.19	4646.43	4043.13	3443.15	2846.39
1.35	5259.64	4653.06	4049.95	3450.17	2853.62
1.40	5267.72	4661.37	4058.50	3458.97	2862.68
1.45	5277.70	4671.62	4069.04	3469.82	2873.85
1.50	5289.84	4684.10	4081.86	3483.00	2887.41
1.55	5304.46	4699.10	4097.27	3498.85	2903.72
1.60	5321.90	4717.00	4115.65	3517.73	2923.14
1.65	5342.53	4738.16	4137.38	3540.06	2946.09
1.70	5366.78	4763.03	4162.90	3566.28	2973.06
1.75	5395.11	4792.08	4192.73	3596.92	3004.57
1.80	5428.04	4825.86	4227.40	3632.56	3041.24
1.85	5466.17	4864.98	4267.59	3673.90	3083.81
1.90	5510.23	4910.22	4314.12	3721.82	3133.26
1.95	5561.15	4962.62	4368.14	3777.68	

Table A.I. (Continued)

T(K)	p(bar)					
	20	21	22	23	24	25
1.20	2242.52	1651.58	1063.58	478.47	-103.80	-683.24
1.25	2246.92	1656.11	1068.25	483.29	-98.83	-678.12
1.30	2252.74	1662.11	1074.44	489.66	-92.25	-671.33
1.35	2260.19	1669.80	1082.36	497.84	-83.81	-662.62
1.40	2269.53	1679.42	1092.29	508.09	-73.24	-651.71
1.45	2281.03	1691.27	1104.51	520.69	-60.24	-638.30
1.50	2295.00	1705.67	1119.35	535.99	-44.46	-622.03
1.55	2311.78	1722.95	1137.16	554.35	-25.53	-602.51
1.60	2331.77	1743.53	1158.37	576.21	-2.99	-579.27
1.65	2355.39	1767.86	1183.43	602.04	23.65	-551.79
1.70	2383.14	1796.43	1212.88	632.42	54.99	-519.45
1.75	2415.57	1829.85	1247.34	667.98	91.72	-481.48
1.80	2453.35	1868.81	1287.56	709.54	134.72	-436.94
1.85	2497.25	1914.15	1334.46	758.14	185.19	-384.34
1.90	2548.37	1967.13				

Table A.I. (Continued)